**NASA Contractor Report** 181815

**ICASE REPORT NO.** 89-18

# ICASE

## INVISCID SPATIAL STABILITY OF A COMPRESSIBLE MIXING LAYER. PART II. THE FLAME SHEET MODEL



T. L. Jackson

C. E. Grosch

Contract Nos. NAS1-18107, NAS1-18605
March 1989

INSTITUTE FOR COMPUTER APPLICATIONS IN SCIENCE AND ENGINEERING
NASA Langley Research Center, Hampton, Virginia 23665

Operated by the Universities Space Research Association

National Aeronautics and
Space Administration

**Langley Research Center**
Hampton, Virginia 23665

# INVISCID SPATIAL STABILITY OF A COMPRESSIBLE MIXING LAYER. PART II. THE FLAME SHEET MODEL

*T. L. Jackson*

Department of Mathematics and Statistics
Old Dominion University
Norfolk, Virginia 23529

*C. E. Grosch*

Department of Oceanography and
Department of Computer Science
Old Dominion University
Norfolk, Virginia 23529

**Abstract.** We report the results of an inviscid spatial stability calculation for a compressible reacting mixing layer. The limit of infinite activation energy is taken and the diffusion flame is approximated by a flame sheet. Results are reported for the phase speeds of the neutral waves and maximum growth rates of the unstable waves as a function of the parameters of the problem: the ratio of the temperature of the stationary stream to that of the moving stream, the Mach number of the moving stream, the heat release per unit mass fraction of the reactant, the equivalence ratio of the reaction, and the frequency of the disturbance. These results are compared to the phase speeds and growth rates of the corresponding nonreacting mixing layer. We show that the addition of combustion has important, and complex, effects on the flow stability.

This work was supported by the National Aeronautics and Space Administration under NASA Contract Nos. NAS1-18107 and NAS1-18605 while the authors were in residence at the Institute for Computer Applications in Science and Engineering, NASA Langley Research Center, Hampton, VA 23665.

**1. Introduction.** Quite recently it has been realized that an understanding of the stability characteristics of compressible mixing layers is extremely important in view of the projected use of the scramjet engine for the propulsion of hypersonic aircraft. For example, Drummond and Mukunda (1988) state: "Even though the combustor flow field is quite complex, it can be realistically viewed as a collection of spatially developing and reacting supersonic mixing layers that are initially discrete, but that ultimately merge into larger more complex zones. These mixing layers begin downstream of a set of fuel injectors that introduce gaseous hydrogen in both a parallel and tranverse direction into a supersonic airstream entering from the engine inlet. The behavior of the initial portion of the combustor flow, in the mixing layers near the fuel injectors, appears to be most critical, since this is where the mechanism for efficient high speed mixing must be established to achieve the required degree of combustion downstream. Because of the structure of the flow field in this initial portion of the combustor, a single supersonic, spatially developing and reacting mixing layer serves as an excellent physical model for the overall flow field." Thus knowledge of the stability characteristics may allow one, in principle, to control the downstream evolution of such flows in the combustor. This is particularly important because of the observed increase in the flow stability at high Mach numbers (Brown and Roshko, 1974; Chinzei, Masuya, Komuro, Murakami, and Kudou, 1986; and Papamoschou and Roshko, 1986). Because of the increase in stability, natural transition may occur at downstream distances which are larger than practical combustor lengths. A number of techniques which may enhance mixing are discussed by Kumar, Bushnell and Hussaini (1987). A detailed understanding of the linear stability characteristics of compressible reacting mixing layers will be of aid in mixing enhancement.

Despite the fact that understanding of the flow field in a reacting compressible mixing layer in a scramjet engine is extremely important, there appears to be very few studies of the stability of such flows. Menon, Anderson and Pai (1984) studied the inviscid spatial stability of a compressible wake in which there was a $H_2$–$O_2$ reaction. These calculations were carried out with a free stream Mach number of 2 and temperature of 1500°K. When the reaction was turned on the flow became completely unstable. The phase speed was found to be a monotonically increasing function of frequency. It seems that their results show a complete absence of neutral or stable disturbances.

The above result appears to be in conflict with that of Drummond and Mukunda (1988). They carried out a numerical simulation using the two dimensional, compressible, time dependent Navier-Stokes equations with combustion in a mixing layer. The reaction was the burning of a 10% $H_2$, 90% $N_2$ fuel in air. The free stream Mach number was taken to be 2, the temperature above and below the plate was 2000°K, and the velocities were 2672 m/s and 1729 m/s above and below the plate, respectively. Because of the expense and difficulty of carrying out these simulations only a few have been done. Drummond and Mukunda found that the nonreacting flow was very stable and that turning on the combustion had little effect. But it should be noted that the authors were not carring out a stability calculation, per se, and did not excite the flow with disturbances with a fixed frequency. They relied on the "natural" disturbances to perturb the flow.

We have begun a systematic study of the stability of compressible mixing layers in which a diffusion flame is embedded. The basic steady flow with which we began is that calculated by Jackson and Hussaini (1988). In their study the limit of infinite activation energy was used and the diffusion flame reduced to a flame sheet. The flame sheet model is a standard approximation and has been used in the study of the burning of a fuel particle in an oxidizing atmosphere and of the flame at the mouth of a tube, for example

(Buckmaster and Ludford, 1982; and Williams,1985). In order to understand the effect of the chemical heat release on the stability of this flow, one must first understand the stability characteristics of the nonreacting flow.

In the first part of our study (Jackson and Grosch, 1989, hereafter referred to as Part I), we considered the inviscid spatial stability problem for the compressible mixing layer with the mean velocity profile approximated by the hyperbolic tangent. We found that there is only a single subsonic neutral mode for two dimensional waves, but that there can be three for three dimensional waves. Beyond a critical Mach number $M_s$, the Mach number at which the phase speed equals that of a sonic wave, the subsonic neutral modes are transformed into supersonic neutral modes which are subsonic at one boundary and supersonic at the other (we have not found any neutral or unstable modes which are supersonic at both boundaries). In addition, another supersonic neutral mode appears at $M_* \geq M_s$, the Mach number at which the sonic speeds of the stationary and moving streams are equal. This supersonic neutral mode has the opposite behavior than the previous at the boundaries. That is, if the continuation of the subsonic neutral mode is supersonic in the moving stream and subsonic in the stationary stream, this new mode is subsonic in the moving stream and supersonic in the stationary stream. Thus, there are always at least two bands of unstable frequencies for Mach numbers greater than $M_*$. One of these bands is a group of fast and the other a group of slow unstable supersonic modes. The fast modes are supersonic with respect to the stationary stream and the slow modes are supersonic with respect to the moving stream. It is important to note that both the fast and slow supersonic modes are vorticity modes and neither of them is an acoustic mode (Mack, 1989). These groups of unstable modes lie in the frequency bands between zero, corresponding to the sonic mode, and the frequency of the supersonic neutral mode. Because these frequency bands always overlap for some range of frequencies, there exist two unstable modes at a fixed Mach number and $\beta_T$ (the ratio of the temperature in the stationary stream to that of the moving stream) for every frequency in this range. The phase speeds of both the fast and slow supersonic modes have a small range about the average, so that little dispersion of wave packets is expected, with a reduction in the dispersion as the Mach number is increased. Three dimensional disturbances show the same general characteristics as two dimensional disturbances. There is always a range of propagation angles for which both the fast and slow unstable modes exist. We also find, in agreement with previous studies, that the maximum growth rate for any $\beta_T$ and M occurs for three dimensional waves. A decrease in $\beta_T$ results in an increase in the growth rate of the unstable waves at any Mach number. An increase in the Mach number at a fixed $\beta_T$ results in a decrease of the growth rates by a factor of three to four up until the Mach number equals $M_*$. For Mach numbers greater than $M_*$, the growth rates of all modes level off and then with increasing Mach number, those of the slow modes begin to increase while those of the fast modes approach a limiting value. However, even at Mach 10, the growth rates of the slow modes are still small compared to those at low subsonic speeds. This, combined with the fact that the unstable waves have little dispersion, is a possible mechanism responsible for the observed increase in the flow stability.

In this paper we report results of a study of the stability of a reacting compressible mixing layer. In section 2 we give the basic equations governing the mean flow and the small amplitude disturbance equations. The boundary conditions and the numerical method are also discussed in this section. Section 3 contains a presentation of our results and conclusions are given in section 4.

**2. The Mean Flow.** The nondimensional equations governing the steady two dimensional flow of a compressible, reacting mixing layer which lies between streams of reactants with different speeds and

temperatures are given by (Jackson and Hussaini, 1988)

$$(\rho U)_x + (\rho V)_y = 0, \qquad 1 = \rho T, \tag{2.1a,b}$$

$$\rho(UU_x + VU_y) = (\mu U_y)_y, \tag{2.1c}$$

$$\rho(UT_x + VT_y) = (\mu T_y)_y + (\gamma-1)M^2\mu U_y^2 + \beta\Omega, \tag{2.1d}$$

$$\rho(UC_{i_x} + VC_{i_y}) = (\mu C_{i_y})_y - \beta_i\Omega, \quad i = 1,2, \tag{2.1e}$$

$$\Omega = D\rho^{a+b+1}C_1^aC_2^be^{-\theta/T}. \tag{2.1f}$$

In these equations the x axis is along the direction of flow, the y axis normal to the flow, $U$ and $V$ are the velocity components in the x and y directions, respectively, $\rho$ is the density, T the temperature, and $C_1$ and $C_2$ the mass fractions. The reaction is assumed to be irreversible and of Arrhenius-type. The viscosity $\mu$ is assumed to be a function of temperature. The other nondimensional parameters appearing above are:

$\beta = QC_{1,\infty}\hat{\nu}W/C_pT_\infty(\hat{\nu}_1 - \hat{\mu}_1)W_1$ — Heat release per unit mass fraction of reactant,

$\theta = E/RT_\infty$ — Activation energy,

$D = \dfrac{l_o}{U_\infty}\dfrac{B\rho_\infty^{a+b}C_{1,\infty}^{a+b-1}\hat{\nu}_1W_1}{W_1^aW_2^b}$ — Damkohler number,

$\beta_i = (\hat{\nu}_i - \hat{\mu}_i)W_i/(\hat{\nu}_1 - \hat{\mu}_1)W_1$ — Parameter involving stoichiometry,

$M = U_\infty/a_\infty$ — Mach number,

where a and b are the reaction orders of $C_1$ and $C_2$, respectively, $\hat{\nu}_j$ the stoichiometric coefficient for species j appearing as a reactant, $\hat{\mu}_j$ the stoichiometric coefficient for species j appearing as a product, $\hat{\nu}$ the sum of the stoichiometric coefficients of the reactants, $W_j$ the molecular weight of species j, W the average molecular weight, E the dimensional activation energy, R the universal gas constant, B the preexponential constant in rate expression, $a_\infty$ the speed of sound referred to $T_\infty$, Q the chemical heat release per unit mass, $\gamma$ the specific-heats ratio, and finally $C_p$ the specific heat at constant pressure. The equations were nondimensionalized by the freestream values $T_\infty$, $\rho_\infty$, $U_\infty$, $C_{1,\infty}$ for the temperature, density, velocities and mass fractions, respectively. Lengths are referred to $l_o$, some characteristic length scale of the flow. We have assumed unit Prandtl and Lewis numbers in writing down these equations. The assumption of unit Lewis number allows us to consider linear combinations of (2.1d) and (2.1e) to eliminate the source term, which then admits similarity-type solutions. For a simplified Hydrogen-Oxygen reaction, typical values of the heat release parameter $\beta$ as a function of the temperature of the moving stream are given in Table 1. Note that as the temperature of the moving stream is increased, $\beta$ is decreased.

We assume that the stream at $+\infty$ is moving, while that at $-\infty$ is stationary. Thus, the boundary conditions consistent with (2.1) are

$$T = U = C_1 = 1\ ,\ C_2 = 0 \qquad as\ y \to \infty, \tag{2.2a}$$

$$T = \beta_T\ ,\ U = 0\ ,\ C_1 = 0\ ,\ C_2 = \frac{C_{2,-\infty}}{C_{1,\infty}} \qquad as\ y \to -\infty. \tag{2.2b}$$

If $\beta_T$ is less than one, the stationary gas is relatively cold compared to the moving stream, and if $\beta_T$ is greater than one it is relatively hot.

The enthalpy for species 1 and 2 is defined by

$$H_i = T + \frac{\beta}{\beta_i} C_i, \quad i = 1,2. \tag{2.3}$$

Combining (2.1d) and (2.1e), and using the boundary conditions (2.2), one finds

$$H_1 = \beta_T + (1 - \beta_T + \beta)U + \frac{\gamma-1}{2} M^2 U(1-U), \tag{2.4a}$$

$$H_2 = \beta_T + \beta\phi^{-1} + (1 - \beta_T - \beta\phi^{-1})U + \frac{\gamma-1}{2} M^2 U(1-U), \tag{2.4b}$$

where $\phi$ is the equivalence ratio, defined by

$$\phi = \frac{C_{1,\infty}/C_{2,-\infty}}{\beta_1/\beta_2}, \tag{2.5}$$

which is the ratio of the mass fraction $C_1$ in the moving stream to the mass fraction $C_2$ in the stationary stream divided by the ratio of their molecular weights times their stoichiometric coefficients. Note that if $\phi = 1$, then the mixture is said to be stoichiometric, and if $\phi > 1$ it is $C_1$ rich, while if $\phi < 1$ it is $C_1$ lean.

A thin diffusion flame exists within the mixing layer and is characterized by near-equilibrium conditions; $C_1 = 0$ on one side of the flame and $C_2 = 0$ on the other. In the limit of infinite activation energy this thin diffusion flame reduces to a flame sheet and from the relations (2.4), we see that the flow can be described by

$$C_1 = 1 - (1 + \phi^{-1})(1-U), \qquad C_2 = 0, \tag{2.6a}$$

$$T = 1 - (1 - \beta_T - \beta\phi^{-1})(1-U) + \frac{\gamma-1}{2} M^2 U(1-U), \tag{2.6b}$$

for $y > y_f$, and

$$C_1 = 0, \qquad C_2 = \frac{\beta_2}{\beta_1}[\phi^{-1} - (1 + \phi^{-1})U], \tag{2.7a}$$

$$T = \beta_T + (1 - \beta_T + \beta)U + \frac{\gamma-1}{2}M^2U(1-U), \tag{2.7b}$$

for $y < y_f$. Here, $y_f$ gives the location of the flame sheet where both reactants vanish, and T takes the adiabatic flame value $T_f$, given by

$$T_f = \beta_T + (1 - \beta_T + \beta)U_f + \frac{\gamma-1}{2}M^2U_f(1-U_f), \tag{2.8}$$

and

$$U_f = U(y_f) = \frac{1}{1+\phi} \tag{2.9}$$

defines the flame location.

The temperature and mass fraction profiles for the steady mean flow have been obtained in terms of the mean flow velocity distribution, $U(y)$. As discussed in Part I, we assume here that

$$U = \frac{1}{2}\,(1 + tanh(\eta)), \tag{2.10}$$

where $\eta$ is the similarity variable and the Howarth-Dorodnitzyn transformation, together with the Chapman linear viscosity law, has been used. This profile satisfies the boundary conditions

$$U \to 1 \quad as \quad \eta \to +\infty, \qquad\qquad U \to 0 \quad as \quad \eta \to -\infty. \tag{2.11}$$

The basic mean flow considered here is thus given by (2.6), (2.7), and (2.10).

In Figure 1a we show plots of $T(\eta)$ for $\beta_T = 2$, $M = 0$, $\phi = 1$ and for various values of the heat release parameter $\beta$. If $\beta$ is different from zero, the temperature always has a discontinuity in its slope at the location of the flame sheet. Figure 1b shows plots of T for $\beta_T = 2$, $\beta = 2$, $M = 0$, and for various values of $\phi$. When $\phi = 1$, the flame sheet is located at $\eta_f = 0$. For $\phi > 1$, the mixture is $C_1$ rich and the flame location shifts to $\eta_f < 0$. For $\phi < 1$, the converse is true. Finally, Figure 1c shows T for various values of the Mach number. As can be seen from (2.6)-(2.8), increasing M increases T. It should be noted that an increase in $\beta$ at fixed M has a qualitatively similar effect on T as an increase in M at a fixed $\beta$.

The flow field is perturbed by introducing two dimensional wave disturbances in the velocity, pressure, temperature, density and mass fractions on either side of the flame sheet with amplitudes which are functions of $\eta$. In addition, the flame sheet location must also be perturbed with a wave disturbance. For example, the pressure perturbation is

$$p = \Pi(\eta)exp[i(\alpha x - \omega t)], \tag{2.12}$$

with $\Pi$ the amplitude. Here, for spatial stability $\alpha$ is complex. The real part of $\alpha$ is the wave number in the x direction, while the imaginary part of $\alpha$ indicates whether the disturbance is amplified, neutral, or damped depending on whether $\alpha_i$ is negative, zero, or positive. The frequency $\omega$ is taken to be real. Substituting the expression (2.12) for the pressure perturbation and similar expressions for the other flow quantities into the inviscid compressible equations yields the ordinary differential equations for the perturbation amplitudes. It is straightforward to derive a single equation governing $\Pi$, given by

$$\Pi'' - \frac{2U'}{U-c}\Pi' - \alpha^2 T[T - M^2(U-c)^2]\Pi = 0, \tag{2.13}$$

which is valid on either side of the flame sheet. Here, c is the complex wave velocity

$$c = \frac{\omega}{\alpha}, \tag{2.14}$$

and primes indicate differentiation with respect to the similarity variable $\eta$. The phase speed, $c_{ph}$, is given by $\omega / \alpha_r$. For a neutral wave the phase speed will be denoted by $c_N$.

The boundary conditions for $\Pi$ are obtained by considering the limiting form of equation (2.13) as $\eta \to \pm\infty$. The solutions to (2.13) are of the form

$$\Pi \to exp(\pm\Omega_{\pm}\eta), \tag{2.15}$$

where

$$\Omega^2_{+} = \alpha^2[1 - M^2(1-c)^2], \qquad \Omega^2_{-} = \alpha^2\beta_T[\beta_T - M^2c^2]. \tag{2.16}$$

Let us define $c_{\pm}$ to be the values of the phase speed for which $\Omega^2_{\pm}$ vanishes. Thus,

$$c_{+} = 1 - \frac{1}{M}, \qquad c_{-} = \frac{\sqrt{\beta_T}}{M}. \tag{2.17}$$

Note that $c_{+}$ is the phase speed of a sonic disturbance in the moving stream and $c_{-}$ is the phase speed of a sonic disturbance in the stationary stream. At

$$M = M_* \equiv 1 + \sqrt{\beta_T} \tag{2.18}$$

$c_{\pm}$ are equal. In addition to the boundary conditions at $\eta = \pm\infty$, we must impose the conditions that $\Pi$ and $\Pi'$ are continuous across the flame sheet.

The nature of the disturbances and the appropriate boundary conditions can now be illustrated by reference to Figure 2, where we plot $c_{\pm}$ versus $M$ for a typical value of $\beta_T$. In what follows we assume that $\alpha^2_r > \alpha^2_i$. These curves divide the $c_r$–$M$ plane into four regions, where $c_r$ is the real part of c. If a disturbance exists with a $M$ and $c_r$ in region 1, then $\Omega^2_{+}$ and $\Omega^2_{-}$ are both positive, and the disturbance is subsonic at both boundaries. In region 3, both $\Omega^2_{+}$ and $\Omega^2_{-}$ are negative and hence the disturbance is supersonic at both boundaries. In region 2, $\Omega^2_{+}$ is positive and $\Omega^2_{-}$ is negative, and the disturbance is subsonic at $+\infty$ and supersonic at $-\infty$, and we classify it as a fast mode. Finally, in region 4, $\Omega^2_{+}$ is negative and $\Omega^2_{-}$ is positive so the disturbance is supersonic at $+\infty$ and subsonic at $-\infty$, and we classify it as a slow mode.

One can now see that the appropiate boundary condition for either damped or outgoing waves in the moving and stationary streams are, respectively,

$$\Pi \to e^{-\Omega_{+}\eta}, \quad \text{if } c_r > c_{+}, \qquad \Pi \to e^{-i\eta\sqrt{-\Omega^2_{+}}}, \quad \text{if } c_r < c_{+}, \tag{2.19a}$$

$$\Pi \to e^{\Omega_{-}\eta}, \quad \text{if } c_r < c_{-}, \qquad \Pi \to e^{-i\eta\sqrt{-\Omega^2_{-}}}, \quad \text{if } c_r > c_{-}. \tag{2.19b}$$

To solve the disturbance equation (2.13), we first transform it to a Riccati equation by setting

$$G = \frac{\Pi'}{\alpha T \Pi}. \tag{2.20}$$

Thus, (2.13) becomes

$$G' + \alpha T G^2 - [\frac{2U'}{U-c} - \frac{T'}{T}]G = \alpha[T - M^2(U-c)^2]. \tag{2.21}$$

The boundary conditions can be found from (2.19) and (2.20), with G continuous across the flame sheet.

The stability problem is thus to solve equation (2.21) for a given real frequency $\omega$ and Mach number M, with U and T defined by (2.10) and (2.6b),(2.7b). In addition to M, the important parameters of this problem are $\beta_T$, $\beta$, and $\phi$. The eigenvalue is the wavenumber $\alpha$. Because this equation has a singularity at $U = c_N$, we shall integrate it along the complex contour (-6,-1) to ($\eta_f$,0) and (6,-1) to ($\eta_f$,0), where $\eta_f$ gives the flame sheet location defined by (2.9). Using a Runge-Kutta scheme with variable step size, we choose an initial $\alpha$ and compute the boundary conditions from (2.19). We then iterate on $\alpha$, using Muller's method, until the boundary conditions are satisfied and the jump in G at ($\eta_f$,0) is less than $10^{-6}$. All calculations were done in 64 bit precision.

**3. Results.** In all of our calculations we have taken $\gamma = 1.4$; $\beta_T = 0.5, 1, 2$; $0 \le \beta \le 5$; $\phi = 0.5, 1, 2$; and $0 \le M \le 10$.

Lees and Lin (1946) have proven that if a neutral mode is to exist in region 1, the phase speed will be given by $c_N = U(\eta_c)$, where $\eta_c$ is found from the regularity condition

$$S(\eta) \equiv \frac{d}{d\eta}(T^{-2}\frac{dU}{d\eta}) = 0. \tag{3.1}$$

The corresponding neutral wave number, $\alpha_N$, must be determined numerically. The eigenfunction is called a subsonic neutral mode. Because $T'$ is discontinuous at $\eta_f$ for nonzero $\beta$, $S(\eta)$ will also be discontinuous at this point. Fiqure 3 is a plot of S versus $\eta$ for various values of $\beta$. As one can see from examination of this figure, S can have a single root, two roots one of which corresponds to $\eta$ positive and the other negative, or two roots one of which is a one-sided zero. The roots of S, which corresponds to phase speeds that are subsonic at both boundaries, are the phase speeds of subsonic neutral modes. The one-sided zero of S may or may not yield a phase speed of a neutral mode. Finally, there can also be singular neutral modes, ones whose phase speeds are not given by (3.1) and are subsonic at the boundaries. If the phase speed corresponding to a zero of S is supersonic at either or both boundaries it may or may not be that of a neutral mode. This can only be determined numerically.

**3.1. M = 0.** The introduction of a chemical reaction, in the form of a flame sheet, has complex effects on the flow stability. In order to show these effects clearly, we first consider the case of zero Mach number and examine the variation of the eigenvalue, $\alpha$, with the heat release parameter $\beta$ and equivalence ratio $\phi$. In Figure 4a we show a plot of the growth rate ($-\alpha_i$) versus the real part of the wavenumber ($\alpha_r$) for the case of $\beta_T = 0.5$, $\phi = 1$, and various values of $\beta$. Note that all of the curves pass through the origin, which corresponds to $\omega = 0$, and also cross the $\alpha_r$ axis, corresponding to $\omega > 0$. These give the two neutral waves. We classify these as true stability curves since the unstable waves are found between two neutral

waves.

The curves shown in Figure 4a are for values of $\beta \leq 0.98$. For this particular set of parameter values we were not able to find solutions to the stability problem whose eigenvalues had the behavior shown in this figure for any values of $\beta > 0.983$. In order to understand the reason for this we carried out an extensive search for eigenvalues in the $\alpha$ plane while varying $\beta$. We discovered that the eigenvalue problem has two unstable solutions for any $\beta > 0$ and the other values of the parameters. Some of these results are shown in Figure 4b. It is clear that there is a saddle point for $\beta$ about 0.984 at $\alpha = 0.24–0.60i$. For $\beta < 0.984$ there are two sets of eigenvalue curves. The lower set appears to be the physically relevant one because it yields the eigenvalue relation for the nonreacting mixing layer as $\beta$ approaches zero. We believe that the upper branch, while corresponding to a correct mathematical solution of the eigenvalue problem, has no physical relevance because none of these upper branch curves intersects the $\alpha_r$ axis and hence there are no neutral solutions ($\alpha_i = 0$) or stable solutions ($\alpha_i > 0$). Similarly, we believe that the solutions on the other two branches, the dashed branches in Figure 4b, are also non-physical because each of them crosses the $\alpha_r$ axis at only one point in the right half plane, that is with $\alpha_r \geq 0$ and hence $c_r > 0$. In other words, these solution branches have only *one* neutral solution with $c_r > 0$ and we therefore believe that these are not physically meaningful solutions. Thus for this set of parameter values, the physically acceptable modes only exist if $0 \leq \beta \leq 0.983$.

We have found similar behavior in the eigenvalue spectrum for other values of the parameters, that is, there is a critical value of $\beta$ ($\beta_c$) beyond which one of the physically acceptable modes no longer exists. This value of $\beta_c$ depends on all of the other parameters of the problem, and the general trends are similar. As $\beta_T$ is increased, $\beta_c$ also increases. Typical values of $\beta_c$ are given in Table 2. The implications, and possible causes, of the existence of $\beta_c$ will be discussed in section 4.

In Figures 5, 6, and 7 we show the variation of the neutral phase speeds $c_N$ with $\beta$ for various values of $\beta_T$ and $\phi$. First, recall that for the nonreactive case (Part I), with $\beta = 0$ and $\phi = 1$, only a single neutral mode exists at $M = 0$, given by (3.1), and is classified as fast or slow depending on whether $c_N > 1/2$ or $c_N < 1/2$, respectively. We will show that the addition of heat release ($\beta > 0$) can cause both fast and slow modes to coexist, although both types may not always exist for all values of $\beta$. Also, there may exist singular neutral modes, those which are found numerically but do not satisfy the regularity condition (3.1). This is in direct contrast to the results of Part I.

It can be shown from (3.1), and from (2.6b), (2.7b) and (2.10), that fast waves only exist for

$$\beta \geq 1 - \beta_T \phi \tag{3.2}$$

with corresponding neutral phase speed

$$c_N = \frac{\beta + \beta_T \phi}{\beta + (1 + \beta_T)\phi}, \tag{3.3}$$

while slow waves only exist for

$$\beta \geq \beta_T \phi - 1 \tag{3.4}$$

with corresponding neutral phase speed

$$c_N = \frac{\beta_T}{1 + \beta + \beta_T}. \tag{3.5}$$

Note that the value of the slow neutral phase speed is independent of the equivalence ratio $\phi$. Also note that there is a mode switch located at $\beta = 0$ and $\phi = \beta_T^{-1}$; i.e., the modes interchange their characteristics at $\beta = 0$.

The phase speeds of the neutral modes for $\beta_T = 0.5$ are plotted in Figure 5. Note that there are both fast and slow subsonic neutral modes whose phase speeds are given by (3.3) and (3.5). In addition, there are both fast and slow singular subsonic neutral modes, adjancent to their corresponding regular neutral modes, whose phase speeds are independent of $\beta$. It is clear from the results shown here that it is the slow modes which cease to exist when $\beta > \beta_c$ and that $\beta_c$ increases with increasing values of the equivalence ratio $\phi$. The fast modes, on the other hand, only exist for those values of $\beta$ which satisfy (3.2). From Figure 5c one can see that there will be a mode switch for $\phi > 2$ at $\beta = 0$. The phase speeds of the neutral modes for $\beta_T = 1$ are plotted in Figure 6. Again we see that there are both fast and slow regular neutral modes with adjacent singular modes. Note that there is a mode switch at $\beta = 0$ as $\phi$ is increased past one. That is, for $\phi < 1$, only the slow modes exist at $\beta = 0$, and conversely for $\phi > 1$. The critical value $\beta_c$, beyond which there are no acceptable solutions, only affects the slower branch. Finally, Figure 7 shows the variation of the phase speed with $\beta$ for $\beta_T = 2$. The mode switch occurs when $\phi$ exceeds 0.5. It is clear that $\beta_c$ is greater than 5 for all values of $\phi$ for which results are shown here.

In addition to the neutral modes there are, of course, associated unstable modes. The maximum growth rates of the unstable modes for various values of $\beta_T$ and $\phi$ are plotted as a function of $\beta$ in Figures 8-10. It is important to note the changes of scale between these figures.

In Figure 8 the variation of $-\alpha_{i_{MAX}}$ with $\beta$ is shown for $\beta_T = 0.5$ and $\phi = 0.5, 1, 2$. The slow modes are much more unstable than the fast modes for those ranges of $\beta$ for which the slow modes exist, i.e. $\beta < \beta_c$. The maximum growth rates of these slow modes first decrease slightly and then increase with an increase in $\beta$. The maximum growth rates of fast modes increase with $\phi$ for any $\beta$ but are much smaller than those of the slow modes. Similar results are shown in Figure 9 for $\beta_T = 1$. The switching between fast and slow modes past $\phi = 1$ which was noted in our discussion of the phase speeds of the neutral modes is apparent in this figure. The growth rates of the fast waves increase with $\phi$, while those of the slow waves decrease. Finally the plots of the maximum growth rate versus $\beta$ for $\beta_T = 2$, shown in Figure 10, have the same general behavior as the two previous figures. That is, there is a mode switch at $\beta = 0$ past $\phi = 1/2$.

The results shown in these figures can be summarized as follows. An increase in $\beta_T$ causes a decrease in the maximum growth rate of the most unstable modes. At fixed $\beta_T$ and $\phi$ the growth rate of the slow modes increases as $\beta$ becomes large, while the growth rate of the fast modes approaches a limiting value. As we shall see, this is the same generic behavior as results from increasing the Mach number while holding all other parameters fixed. Thus, for sufficiently large $\beta$, the slow modes are the most unstable ones. For fixed $\beta$, an increase in $\phi$ causes an increase in the maximum growth rates of the fast modes, while decreasing the maximum growth rates of the slow modes. Finally, as in Part I we have found that the phase speeds $c_{ph}$ of the unstable modes lie between the phase speed of the regular neutral mode and its adjacent singular neutral mode.

**3.2. M > 0.** In this section we show the variation of the phase speeds of the neutral waves and the maximum growth rates of the unstable waves as a function of the Mach number for various combinations of $\beta_T$, $\beta$, and $\phi$.

In Figure 11a we show the phase speed of the neutral modes for the nonreactive ($\beta = 0$, $\phi = 1$) mixing layer (Part I) for $\beta_T = 1/2$. From this figure, taken from Part I, one can see that there is only a single subsonic neutral mode in region 1. This mode crosses over the sonic curve at $M_s$, the Mach number at which the phase speed equals that of a sonic wave, and is transformed into a supersonic neutral mode in region 4. In addition, a fast supersonic neutral mode appears at $M_*$ in region 2. In regions 2 and 4 there are unstable modes with phase speeds between that of the supersonic neutral mode and that of the sonic neutral mode. Thus, there are two bands of unstable frequencies for Mach numbers greater than $M_*$. The band in region 2 is a group of fast and the band in region 4 is a group of slow unstable modes. The phase speeds of both the fast and slow modes have a small range about the average, so that little dispersion of wave packets is expected, with a reduction in the dispersion as the Mach number is increased.

It can be seen from Figure 11b that chemical reaction has a major effect on $c_N$. First, recall from Figure 5b that the slow subsonic neutral mode only exists for $\beta < \beta_c$ at $M = 0$, while the fast subsonic neutral mode only exists for $\beta \geq 1/2$. As can be expected, the value of $\beta_c$ is also a function of the Mach number. Thus, we find that the slow neutral mode only exists if the Mach number is greater than the critical value $M_c$ (see Figure 11b). Apart from this the values of $c_N$ on this branch are only slightly affected by changes in $\beta$ and the effect is quite small at large M. Finally, one can see that a fast subsonic neutral mode is present for all M because $\beta$ is greater than 0.5. Note that the values of $c_N$ for this fast mode in region 1 increase markedly with increasing $\beta$. This is also true for the lower Mach number range in region 2, but all of the $c_N$ curves for different $\beta$ appear to asymptote to a single curve for large M. Associated with the fast and slow modes there are singular subsonic neutral modes in region 1. The range of phase speeds of the unstable modes in region 1 lies between the fast modes and their associated singular mode, and between the slow modes and their associated singular mode. In regions 2 and 4, the range of phase speeds of the unstable modes lies between the fast (slow) supersonic neutral modes and the associated fast (slow) sonic neutral modes. The range of the phase speeds of the unstable modes increases with $\beta$ and is quite large for Mach numbers around $M_*$, thus yielding an increase in dispersion. However for Mach numbers much larger than $M_*$ the dispersion is essentially independent of $\beta$.

Figure 12 shows the phase speed of the neutral modes for $\beta_T = 1$, $\phi = 1$ and various values of $\beta$ as a function of the Mach number. The results for $\beta = 0$ are shown in Figure 12a and those for $\beta > 0$ in Figure 12b. The curves of $c_N$ versus M are symmetric about the line $c_N = 1/2$ because the mean velocity profile is symmetric about $\eta = 0$ (where $U = 1/2$) and so is the temperature profile for any $\beta$ if $\phi = 1$. Hence, the subsonic neutral mode in region 1 of Figure 12a splits into a symmetric pair of fast and slow supersonic modes at $M_*$. From Figure 12b at can be seen that this is also true for any nonzero $\beta$. The only exception is for sufficiently large $\beta$, where the slow neutral modes only exist if the Mach number exceeds $M_c$. For this case, the singular subsonic mode in region 1 has a phase speed of 1/2, and the range of phase speeds of the unstable modes lies between this mode and the corresponding fast and slow neutral modes. As $\beta$ increases the phase speeds of the fast (slow) neutral modes increase (decrease) at any fixed M. Again it should be noted that all of the curves for both the fast and slow neutral modes at different $\beta$ are asymptotic to a single curve for large M. As for the previous case, an increase in $\beta$ causes an increase in the range of the phase speeds of the unstable modes, in the vicinity of $M_*$, and hence an increase in the dispersion.

Finally, in Figure 13 we show similar plots of $c_N$ versus M for $\beta_T = 2$. In Figure 13a, with $\beta = 0$, there is only a subsonic fast neutral mode in region 1 which is transformed into a supersonic neutral mode in region 2. The slow supersonic neutral mode only exists in region 4. The effects of increasing $\beta$ are similiar to those of the cases discussed above. There is an increase in the phase speed of the fast modes as $\beta$ is increased. The phase speed of the slow supersonic modes of region 4 decreases with increasing $\beta$ and, for $\beta > 1$, a singular subsonic neutral mode with $c_N = 1/2$ appears in region 1. Correspondingly, for $\beta > 0$, there also exists a singular subsonic neutral mode in region 1 associated with the fast modes. Again the curves for the fast and slow neutral modes are each asymptotic to a single curve for large M. As in the previous two cases, an increase in $\beta$ causes an increase in the range of the phase speeds of the unstable waves and hence an increase in the dispersion.

We have also carried out calculations of $c_N$ versus M for fixed $\beta_T$ and $\beta$ with various values of $\phi$. The results can be easily summarized. As $\phi$ increases the phase speed of the slow mode is unchanged, consistent with the Mach zero results (see equation 3.5). The only effect is a change in the critical value of $M_c$ below which this neutral mode does not exist; the smaller the value of $\phi$ the larger is the value of $M_c$. The phase speed of the fast neutral modes decreases with increasing $\phi$. Finally, all of these curves appear to be asymptotic to a single curve as $M \to \infty$.

In addition to the phase speeds we have calculated the maximum growth rates of the unstable modes for these values of $\beta_T$, $\beta$, and $\phi$ as a function of the Mach number. The results are shown in Figures 14-16. Again, it is important to note the changes of scales between these figures.

The maximum growth rate as a function of M with $\beta_T = 1/2$, $\phi = 1$ and various $\beta$ is plotted in Figure 14a. For $\beta = 0$ an increase in the Mach number from zero results in a decrease in the growth rate of the slow mode by a factor of three to four up to $M_*$, and for higher Mach numbers the growth rate levels off and eventually begins to increase with increasing Mach number. An increase in $\beta$ causes the growth rate of the slow modes to increase, but the variation of the growth rate with M is similar to that for $\beta = 0$. However it must be recalled that, if $\beta > 0$, the slow modes only exist for Mach numbers greater than $M_c$, and this is reflected in the curves for $\beta > 0.983$. The growth rates of the fast modes are much smaller and increasing $\beta$ has only a slight effect on them. Figure 14b contains similar results, but with $\beta = 2$ and varying $\phi$. An increase in $\phi$ causes an increase in the maximum growth rate of the slow modes and a decrease for the fast modes at low and moderate Mach numbers. At higher Mach numbers, the growth rates are essentially independent of $\phi$.

Similar results, but with $\beta_T = 1$, are given in Figure 15. It can be seen that the effects of varying $\beta$ on the growth rate (Figure 15a) is somewhat more complex than for the previous case. The maximum growth rate of the slow modes at low Mach numbers first decreases and then increases with increasing $\beta$, consistent with the Mach zero results of Figure 9. At higher Mach numbers, increasing $\beta$ causes a monotonic increase in the maximum growth rates of the slow modes. Again there is a three to four fold decrease in the growth rates of the slow modes as the Mach number increases from zero to $M_*$, and a slight increase at higher Mach numbers. Apart from the appearance of the fast modes at low Mach number, increasing $\beta$ has little effect on their maximum growth rates. Finally, in Figure 15b, an increase in $\phi$ with fixed $\beta$ results in an increase in the maximum growth rate of the fast modes and a decrease in the maximum growth rate of the slow modes at low and moderate Mach numbers. At higher Mach numbers, the growth rates are again independent of $\phi$.

In Figure 16 similar results are given for $\beta_T = 2$. These results are consistent with the Mach zero results of Figure 10. In particular, Figure 16a shows that the slow modes are strictly increasing and those of the fast modes are strictly decreasing with increasing $\beta$ at zero Mach number. Thus, increasing $\beta$ causes a substantial decrease in the maximum growth rates of the fast modes and a substantial increase in the maximum growth rates of the slow modes at low and moderate Mach numbers. As in the previous case, the results of Figure 16b show that increasing $\phi$ yields an increased in the growth rates of the fast modes while decreasing those of the slow modes. As before, the growth rates of both are independent of $\phi$ at higher Mach number.

The results presented in Figures 14-16 thus show that the maximum growth rates of the slow modes increase as the Mach number becomes large, while that of the fast modes approaches a limiting value. As we have seen, this was the same generic behavior as results from increasing the heat release parameter $\beta$ at zero Mach number.

Figures 17 thru 20 are plots of selected two dimensional neutral eigenfunctions for $\beta_T = 1$, $\phi = 1$, Mach 5 and increasing values of $\beta$. These plots show the variation of $\Pi$ with $\eta_r$ on the contour $\eta_i = -1$. All of these have been normalized so that the maximum of the absolute value of $\Pi$ is unity. The eigenfunctions shown are all fast supersonic neutral modes. Note the rapid variation of both the amplitude and phase near $\eta_r = 0$. Because these modes are fast, they show exponential decay in the subsonic region and oscillations with constant amplitude and linear phase in the supersonic region. As $\beta$ is increased, the variation of the amplitude near $\eta_r = 0$ increases markedly. Also, the decay of the amplitude in the subsonic region is more rapid and the rate of change of the phase in the supersonic region increases. The behavior of the eigenfunction with increasing heat release, $\beta$, is similar to the behavior with increasing Mach number.

**4. Conclusions.** The addition of combustion in the form of a flame sheet has important, and complex, effects on the flow stability. In contrast to the nonreacting case, we have shown the existence of multiple regular and singular subsonic neutral modes in region 1. For Mach numbers greater than $M_*$, there are two bands of unstable frequencies (just as in the nonreacting case); one a group of fast supersonic modes and the other a group of slow supersonic modes. In general, an increase in $\beta$ causes an increase (decrease) in the phase speed of the fast (slow) neutral modes. Since the range of phase speeds is increased at low and moderate Mach numbers as the heat release parameter $\beta$ is increased, there is an increase in the dispersion of wave packets. Finally, we have found that the addition of chemical heating has almost no effect on the phase speeds at higher Mach numbers.

The maximum growth rates of the unstable modes decrease by a factor of three to four as the Mach number approaches $M_*$, even with the presence of the reaction. Just as in the nonreacting case, for Mach numbers greater than $M_*$, the growth rates level off and those of the slow modes eventually begin to increase with increasing Mach number, while the growth rates of the fast modes approaches a limiting value. The same behavior results from increasing $\beta$ while the Mach number is held fixed. Finally, if the stationary gas is colder than the moving gas, $\beta_T < 1$, the effect of increasing the equivalence ratio $\phi$ is to increase the growth rate of the slow modes and decrease the growth rate of the fast modes. On the other hand, if $\beta_T \geq 1$, increasing $\phi$ has the opposite effect. However, at higher Mach numbers, changes in $\phi$ have little effect on the growth rates for any $\beta_T$. Finally, an examination of the eigenfunctions shows that increasing $\beta$ has the same generic effect as increasing the Mach number.

As was discussed in section 3.1, we found that with $\beta_T = 1/2$, $\phi = 1$, and $M = 0$ there was a saddle point in the complex $\alpha$ plane for $\beta$ about 0.984. For any $\beta > 0$ there were two branches of $\alpha$. As was discussed in that section, we accepted only that branch which yielded the eigenvalue relation for the nonreacting mixing layer as $\beta$ approached zero. Similar behavior was also found for other values of $\beta_T$ and Mach numbers, but generally the saddle point appeared at larger values of $\beta$. Thus, one can conclude that there will be a value of $\beta$ beyond which one of the branches ceases to have physically meaningful solutions to the stability problem. We suspect that this is due to the use of the flame sheet approximation. In this model, although T is continuous everywhere, $T'$ is discontinuous across the flame sheet and the magnitude of the jump in $T'$ increases with $\beta$. If we are correct, the activation energy $\theta$ must be taken to be large but finite.

This study is the only comprehensive study, of which we know, of the inviscid spatial stability of a reacting compressible mixing layer. We do not know how sensitive our results are to the assumptions used in this study. In particular, we have assumed unit Prandtl and Lewis numbers, used Chapman's linear relation between viscosity and temperature, and approximated the mean velocity profile by a hyperbolic tangent. In addition, we have taken the limit of infinite activation energy which reduces the diffusion flame to a flame sheet. Despite these limitations, we believe that this systematic study is an important first step in classifying and understanding the complex effects that chemistry has on the stability of compressible free shear layers. As mentioned above, the next step is to consider a more realistic model of the chemistry and the thermodynamics. This will then yield mean velocity, temperature, and mass fraction distributions which will be continuous and have continuous derivatives across the flame. However the calculation of the mean field as well as the perturbation solution will be more difficult since now the velocity, temperature, and mass fraction equations are coupled. We have begun this study with large, but finite $\theta$, and hope to report the results at a later date and will compare those results to the benchmark results reported here.

**Acknowledgements.** We wish to acknowledge helpful conversations and comments from J. P. Drummond.

## REFERENCES

Brown, G. L. & Roshko, A. 1974 On Density Effects and Large Structure in Turbulent Mixing Layers. J. Fluid Mech., 64, pp. 775-816.

Buckmaster, J. D. & Ludford, G. S. S. 1982 *Theory of Laminar Flames*. Cambridge University Press, Cambridge.

Chinzei, N., Masuya, G., Komuro, T., Murakami, A. & Kudou, D. 1986 Spreading of Two-Stream Supersonic Turbulent Mixing Layers. Phys. Fluids, 29, pp. 1345-1347.

Drummond, J. P. & Mukunda, H. S. 1988 A Numerical Study of Mixing Enhancement in Supersonic Reacting Flow Fields. AIAA Paper 88-3260.

Jackson, T. L. & Grosch, C. E. 1989 Inviscid Spatial Stability of a Compressible Mixing Layer. J. Fluid Mech., Accepted for publication. Also, ICASE Rep. No. 88-33.

Jackson, T. L. & Hussaini, M. Y. 1988 An Asymptotic Analysis of Supersonic Reacting Mixing Layers. Comb. Sci. Tech., 57, pp. 129-140.

Kumar, A., Bushnell, D. M. & Hussaini, M. Y. 1987 A mixing augmentation technique for hypervelocity scramjets. AIAA Paper No. 87-1882.

Lees, L. & Lin, C. C. 1946 Investigation of the stability of the laminar boundary layer in a compressible fluid. NACA Tech. Note 1115.

Mack, L. M. 1989 On the inviscid acoustic-mode instability of supersonic shear flows. Fourth Symposium on Numerical and Physical Aspects of Aerodynamic Flows, California State University, Long Beach, California.

Menon, S., Anderson, J. D. and Pai, S. I. 1984 Stability of a Laminar Premixed Supersonic Free Shear Layer With Chemical Reactions. Int. J. Engng. Sci., 22(4), pp. 361-374.

Papamoschou, D. & Roshko, A. 1986 Observations of supersonic free-shear layers. AIAA Paper No. 86-0162.

Williams, F. A. 1985 *Combustion Theory*, 2nd Ed., The Benjamin/Cummings Pub. Co., Menlo Park, Ca.

| $T_\infty$ ($K^o$) | $C_P$ (cal/mole $K^o$) | $Q\hat{\nu}W/\hat{\nu}_1 W_1$ (kcal/mole) | $\beta$ |
|---|---|---|---|
| 1000 | 9.03 | 516.5 | 3.2 |
| 1500 | 9.94 | 516.5 | 1.9 |
| 2000 | 10.60 | 516.5 | 1.4 |

Table 1. Typical values of the heat release parameter $\beta$ as a function of temperature.

| $\beta_T$ | $\phi$ 0.5 | 1.0 | 2.0 |
|---|---|---|---|
| 0.5 | 0.7 | 0.984 | 1.8 |
| 1.0 | 2.0 | 3.1 | >5 |
| 2.0 | >5 | >5 | >5 |

Table 2. Typical values of $\beta_c$ at $M = 0$ as a function of $\beta_T$ and $\phi$.

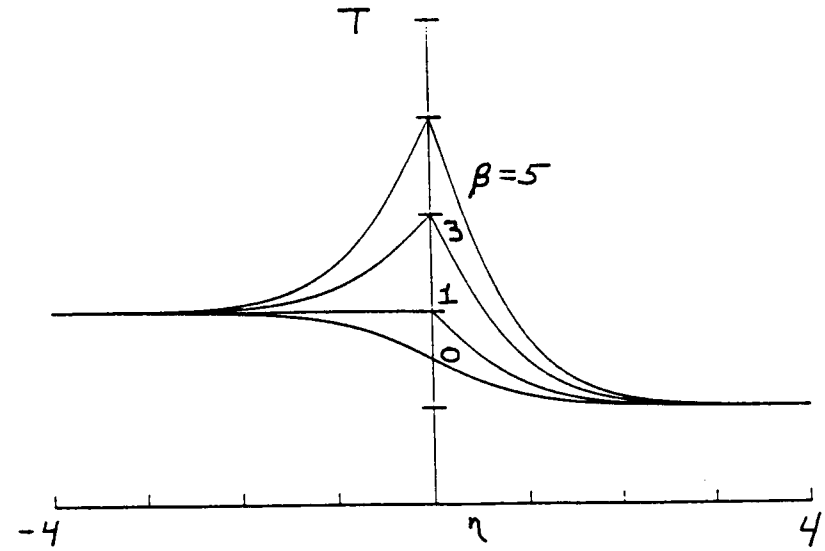


Figure 1a. Plot of temperature T versus $\eta$ for $\beta_T = 2$, $\beta = 0, 1, 3, 5$, $\phi = 1$, and $M = 0$.

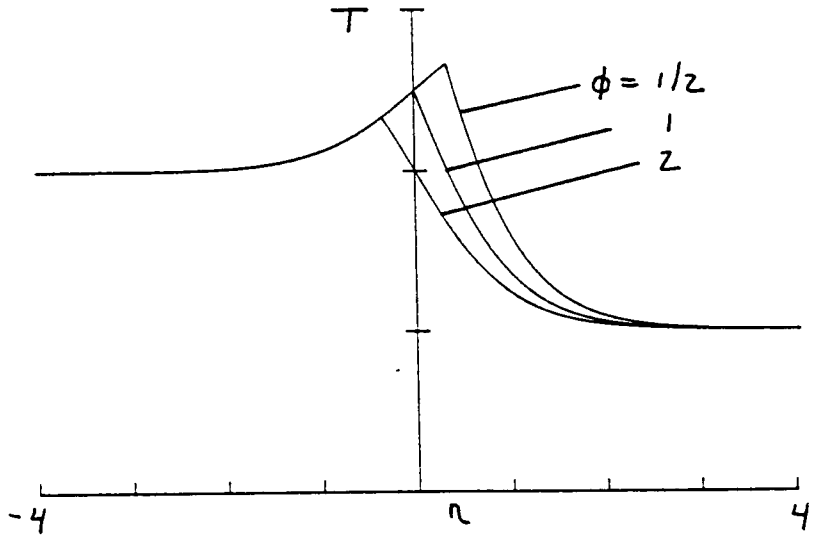


Figure 1b. Plot of temperature T versus $\eta$ for $\beta_T = 2$, $\beta = 2$, $\phi = 0.5, 1, 2$, and $M = 0$.

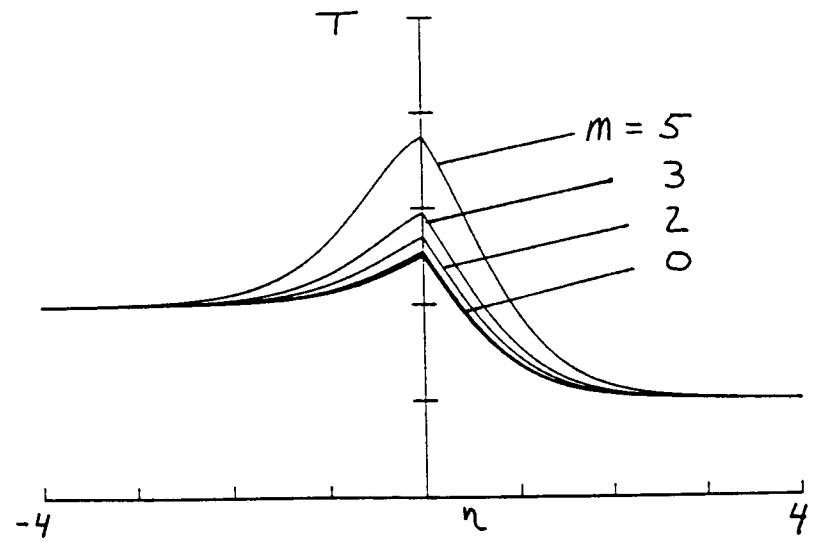


Figure 1c. Plot of temperature T versus $\eta$ for $\beta_T = 2$, $\beta = 2$, $\phi = 1$, and $M = 0, 2, 3, 5$.

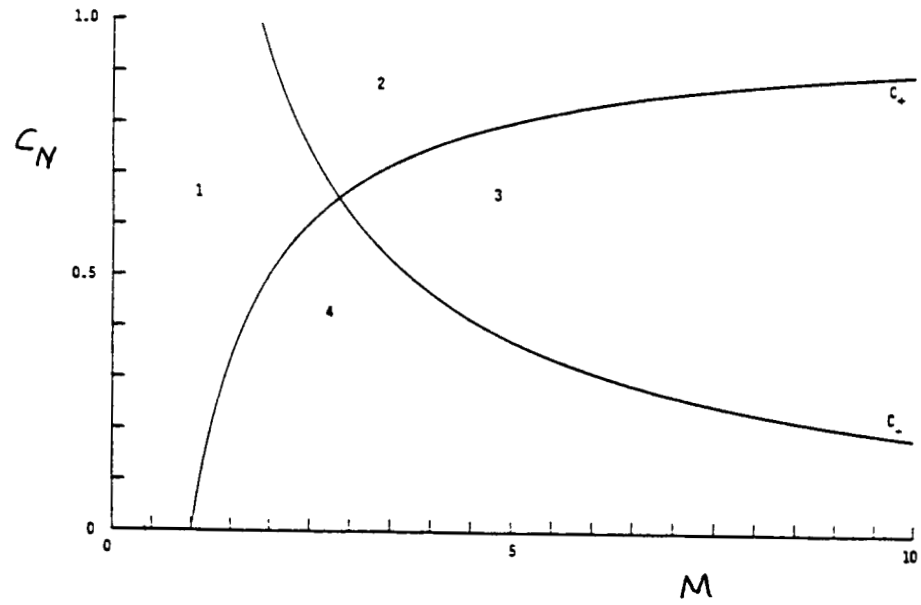


Figure 2. Plot of the sonic speeds $c_{\pm}$ versus Mach number for $\beta_T = 3.5$.

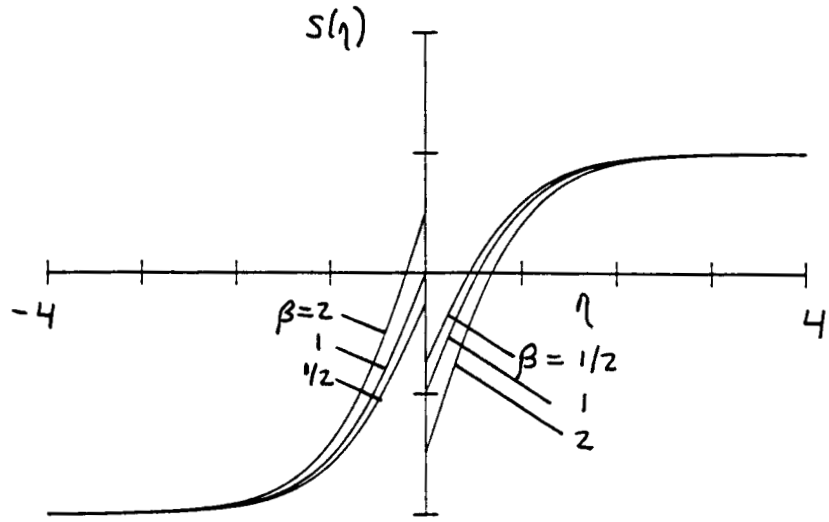


Figure 3. Plot of $S(\eta)$ for $\beta_T = 2$, $\beta = 0.5, 1, 2$, $\phi = 1$, and $M = 0$.

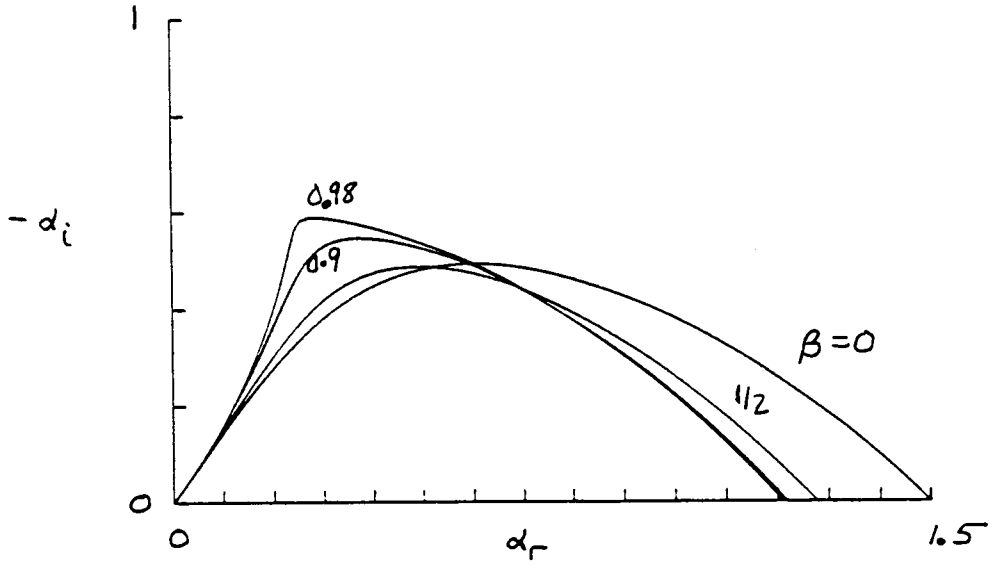


Figure 4a. Plot of the growth rate ($-\alpha_i$) versus the real part of the wavenumber ($\alpha_r$) for $\beta_T = 0.5$, $\beta = 0, 0.5, 0.9, 0.98$, $\phi = 1$, and $M = 0$.

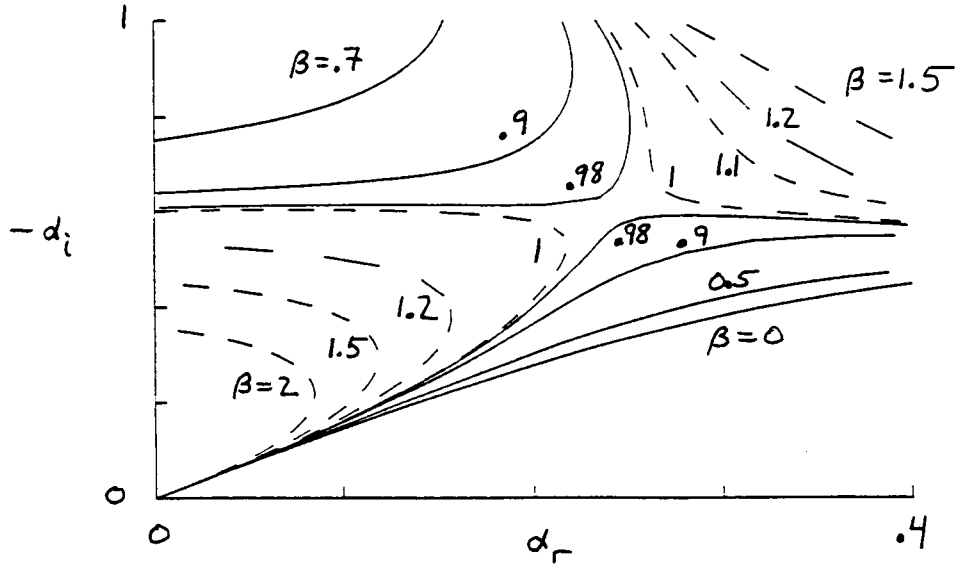


Figure 4b. Plot of the growth rate ($-\alpha_i$) versus the real part of the wavenumber ($\alpha_r$) for $\beta_T = 0.5$, $\phi = 1$, $M = 0$, and various values of $\beta$ showing the saddle point location.

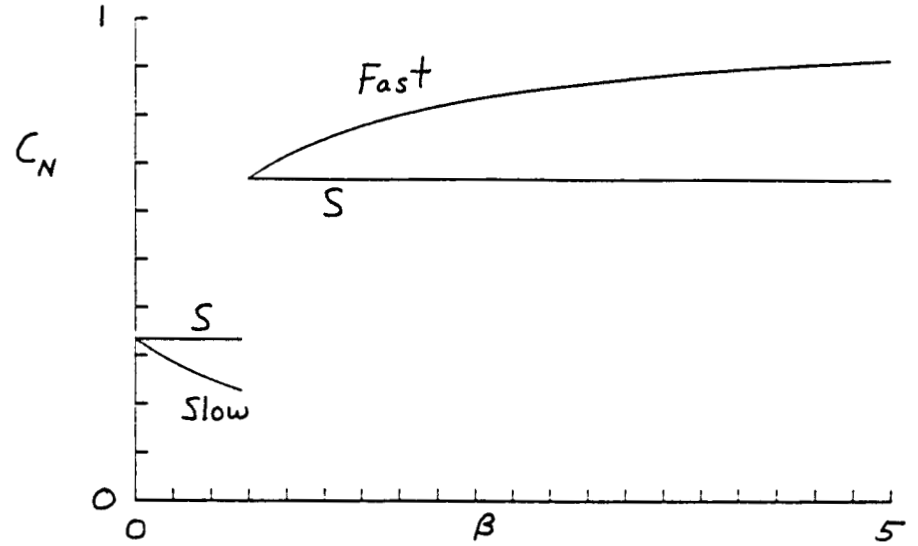


Figure 5a. Plot of neutral phase speeds $c_N$ versus β for $\beta_T = 0.5$, $\phi = 0.5$, and $M = 0$.

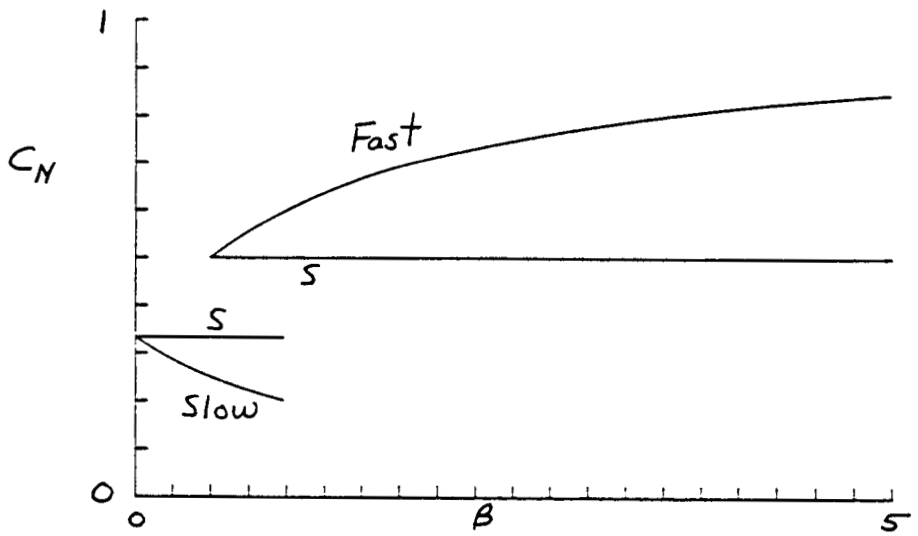


Figure 5b. Plot of neutral phase speeds $c_N$ versus β for $\beta_T = 0.5$, $\phi = 1$, and $M = 0$.

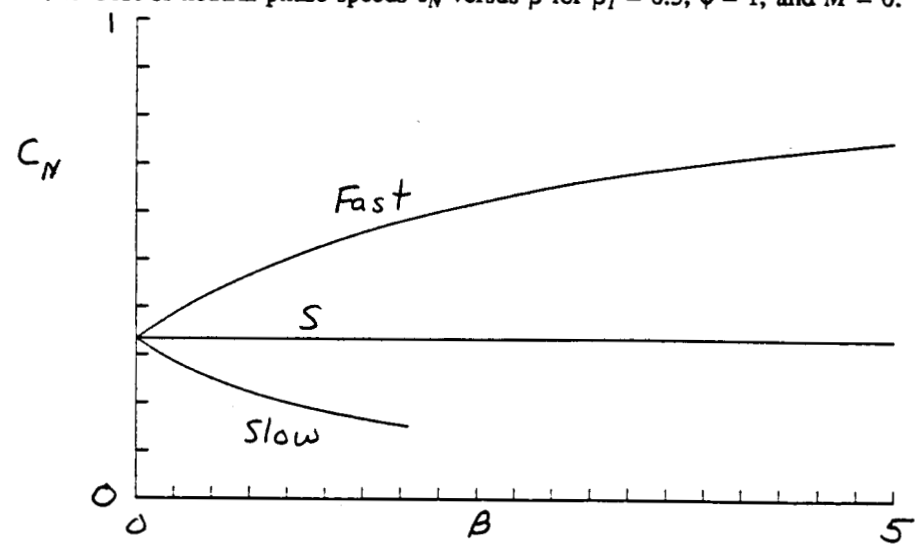


Figure 5c. Plot of neutral phase speeds $c_N$ versus β for $\beta_T = 0.5$, $\phi = 2$, and $M = 0$.

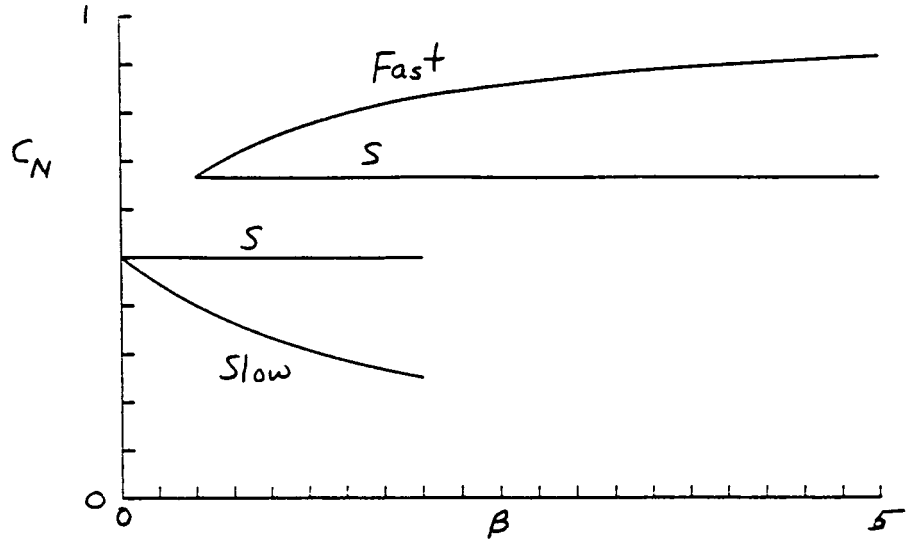


Figure 6a. Plot of neutral phase speeds $c_N$ versus β for $\beta_T = 1$, $\phi = 0.5$, and $M = 0$.

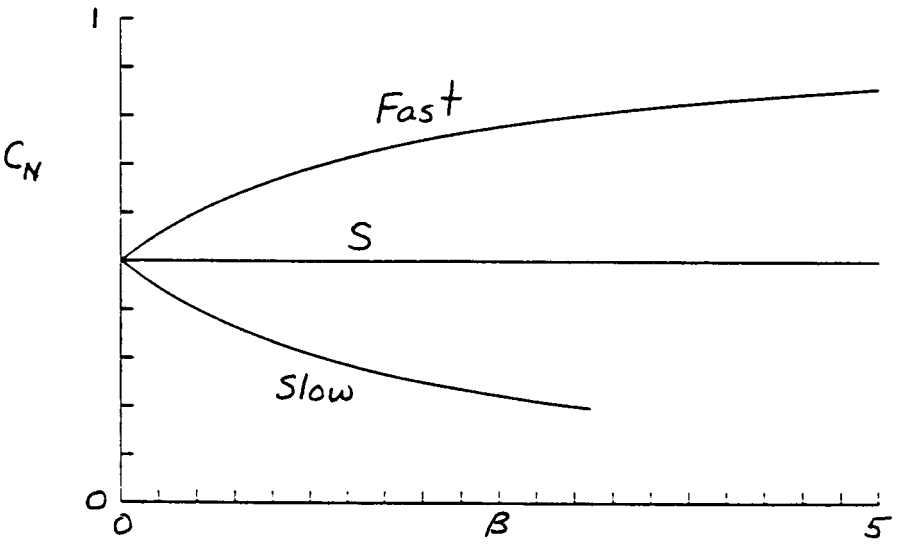


Figure 6b. Plot of neutral phase speeds $c_N$ versus β for $\beta_T = 1$, $\phi = 1$, and $M = 0$.

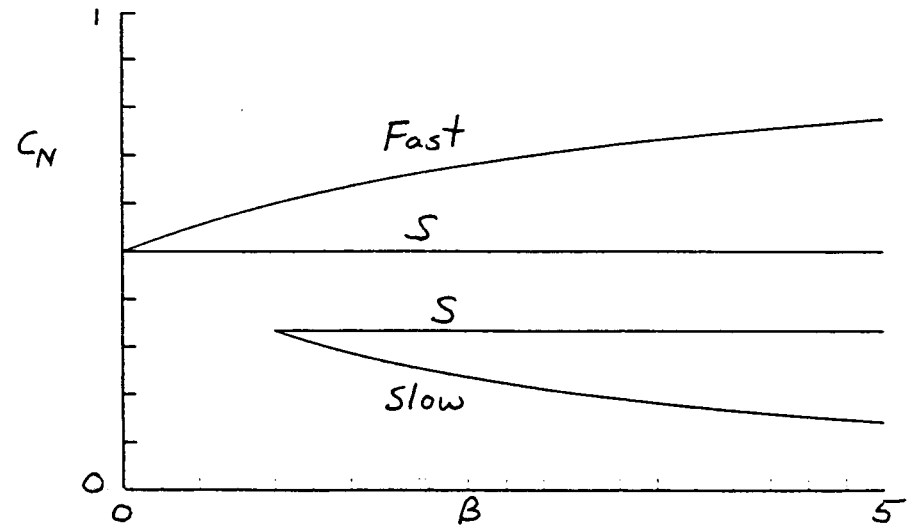


Figure 6c. Plot of neutral phase speeds $c_N$ versus β for $\beta_T = 1$, $\phi = 2$, and $M = 0$.

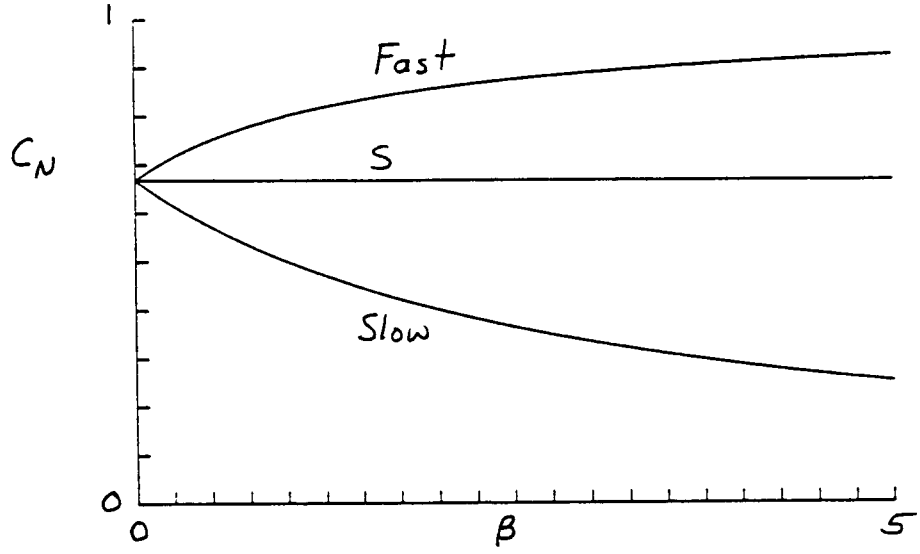


Figure 7a. Plot of neutral phase speeds $c_N$ versus β for $\beta_T = 2$, $\phi = 0.5$, and $M = 0$.

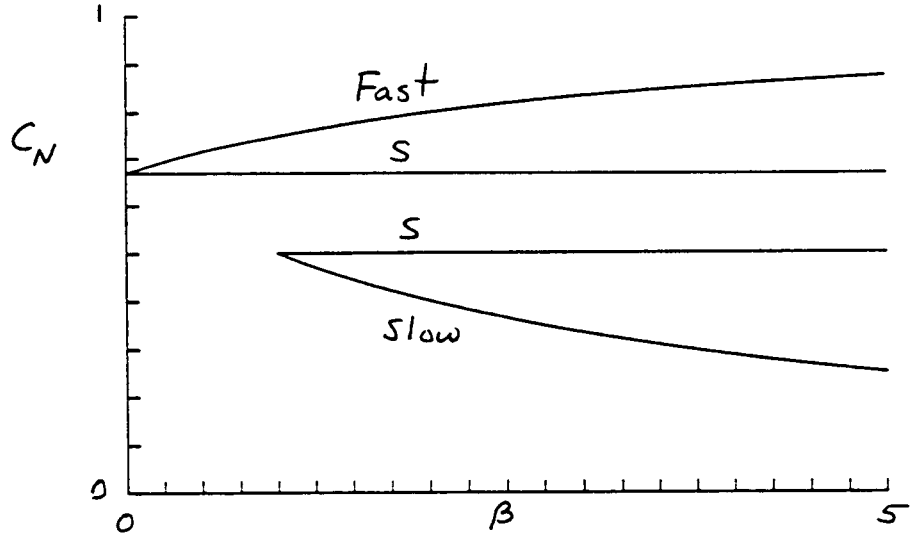


Figure 7b. Plot of neutral phase speeds $c_N$ versus β for $\beta_T = 2$, $\phi = 1$, and $M = 0$.

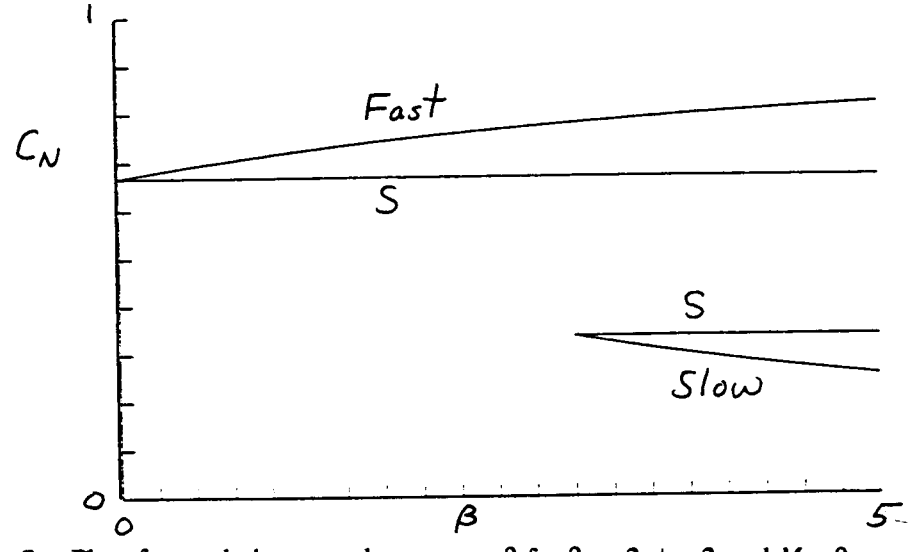


Figure 7c. Plot of neutral phase speeds $c_N$ versus β for $\beta_T = 2$, $\phi = 2$, and $M = 0$.

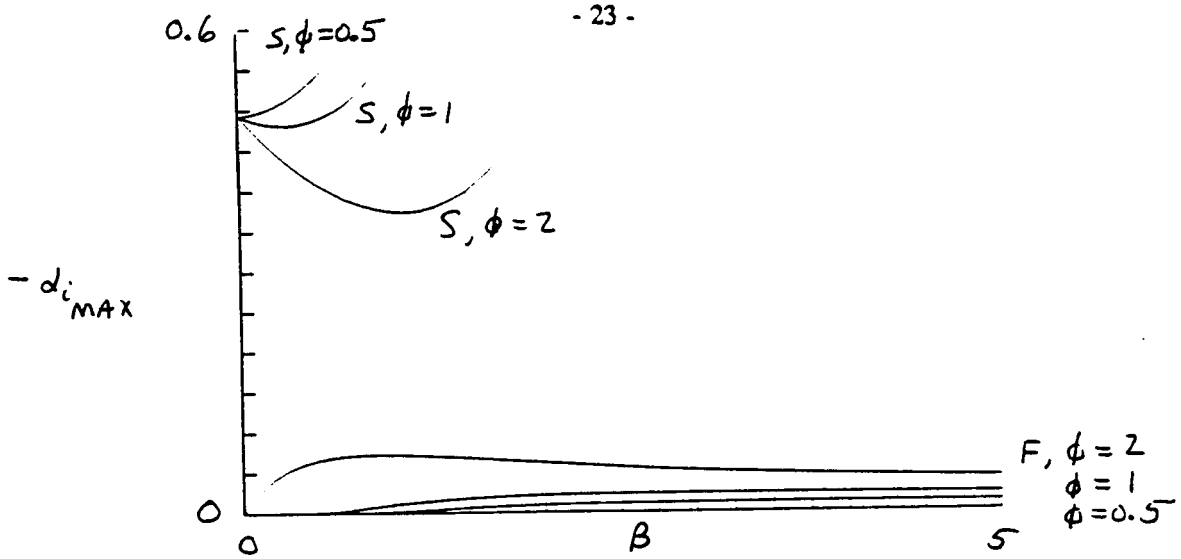


Figure 8. Plot of maximum growth rates of the fast and slow modes versus β for $\beta_T = 0.5$, $\phi = 0.5$, 1, 2, and $M = 0$.

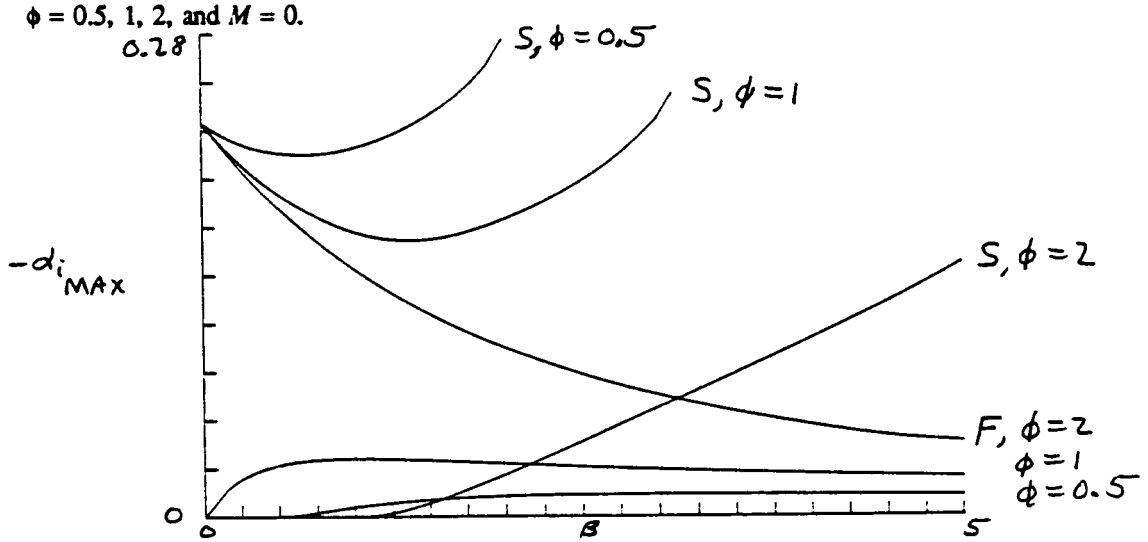


Figure 9. Plot of maximum growth rates of the fast and slow modes versus β for $\beta_T = 1$, $\phi = 0.5$, 1, 2, and $M = 0$.

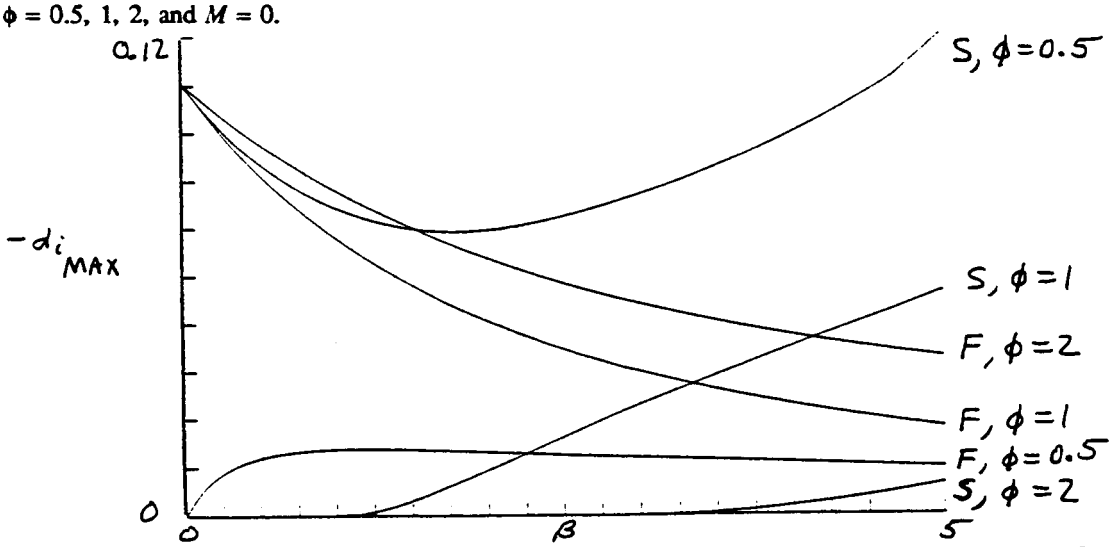


Figure 10. Plot of maximum growth rates of the fast and slow modes versus β for $\beta_T = 2$, $\phi = 0.5$, 1, 2, and $M = 0$.

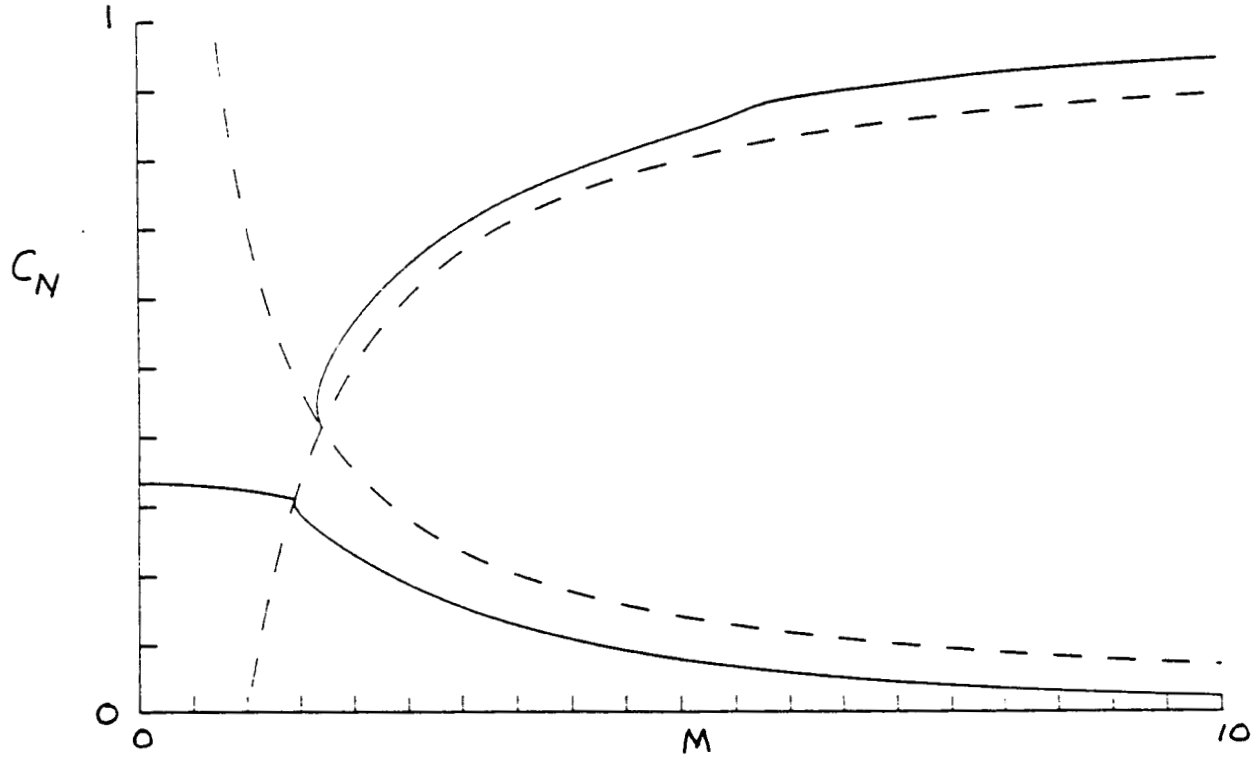


Figure 11a. Plot of neutral phase speeds (solid) and sonic speeds (dashed) versus Mach number for $\beta_T = 0.5$, $\beta = 0$, and $\phi = 1$.

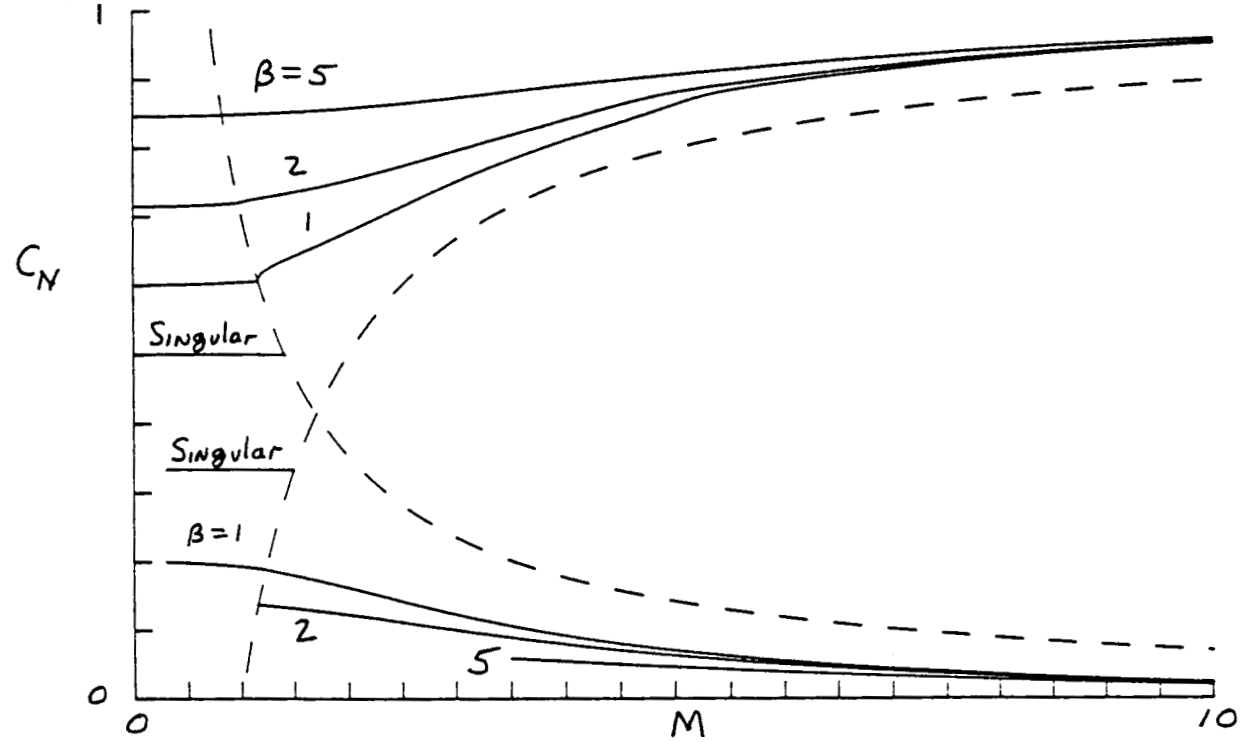


Figure 11b. Plot of neutral phase speeds (solid) and sonic speeds (dashed) versus Mach number for $\beta_T = 0.5$, $\beta = 1, 2, 5$, and $\phi = 1$.

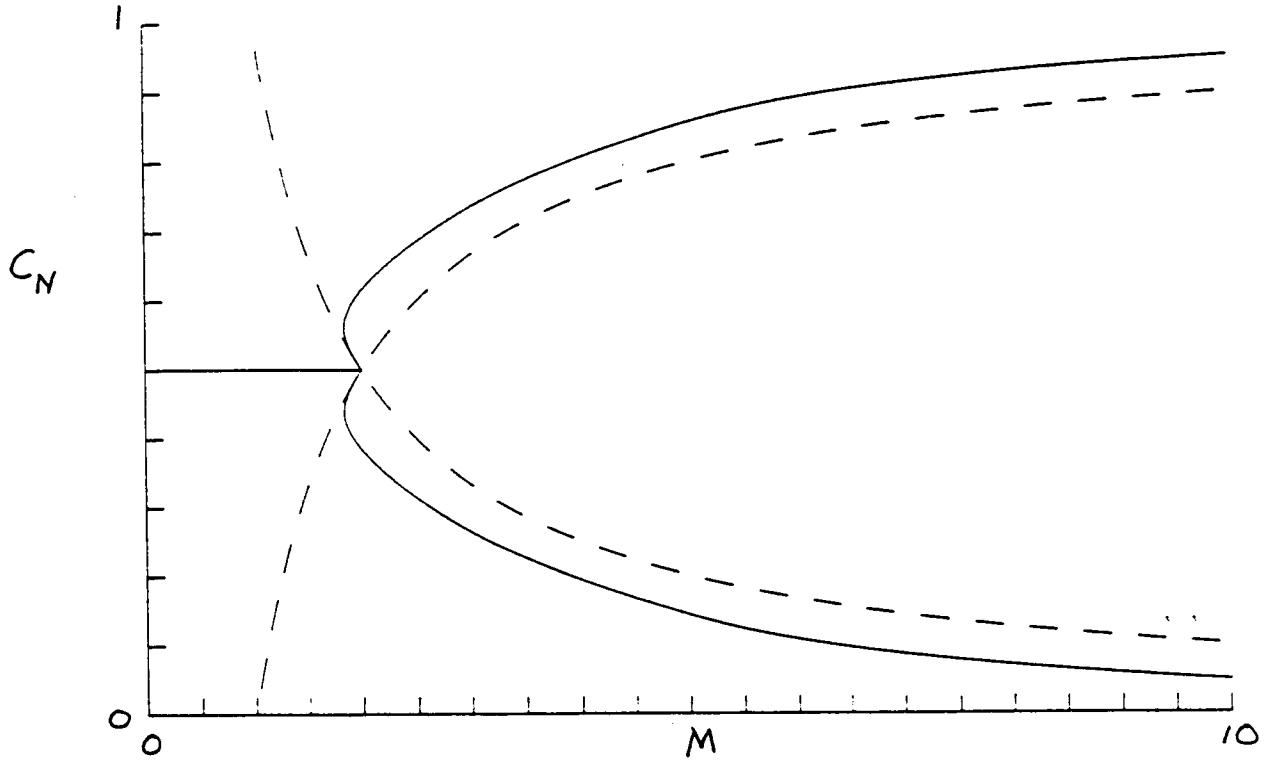


Figure 12a. Plot of neutral phase speeds (solid) and sonic speeds (dashed) versus Mach number for $\beta_T = 1$, $\beta = 0$, and $\phi = 1$.

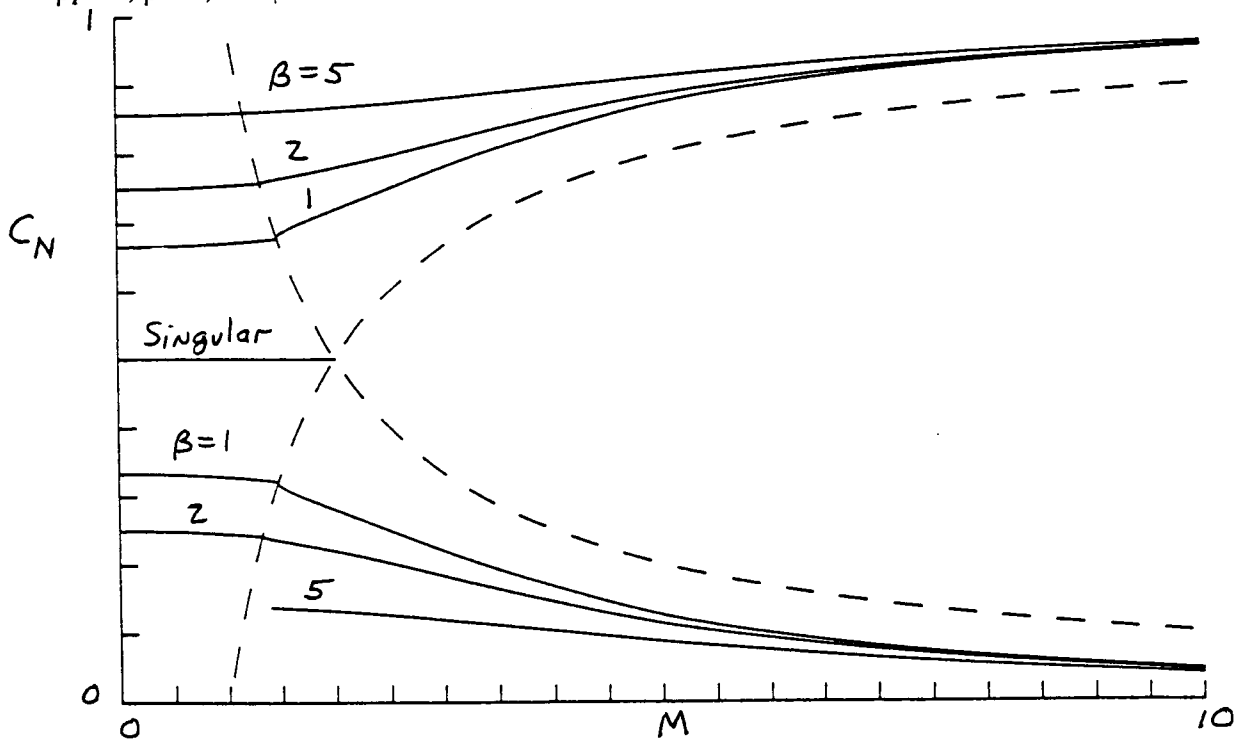


Figure 12b. Plot of neutral phase speeds (solid) and sonic speeds (dashed) versus Mach number for $\beta_T = 1$, $\beta = 1, 2, 5$, and $\phi = 1$.

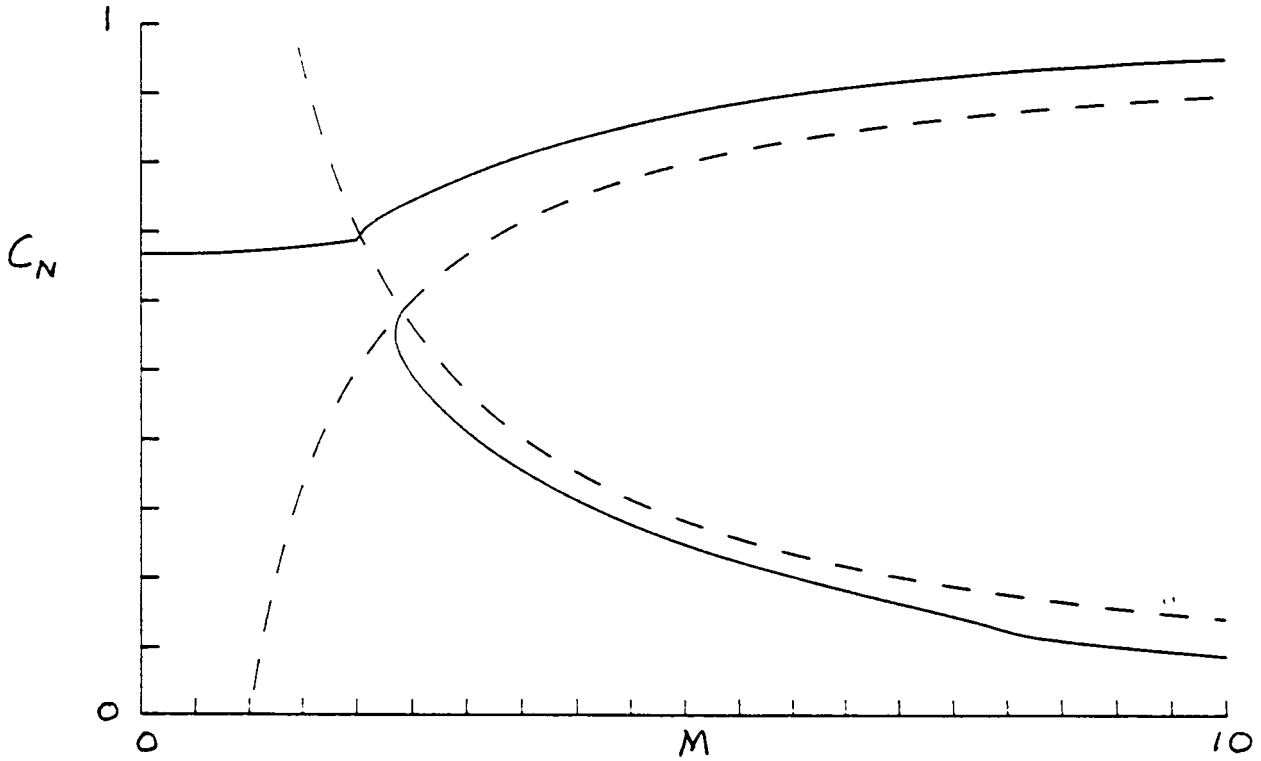


Figure 13a. Plot of neutral phase speeds (solid) and sonic speeds (dashed) versus Mach number for $\beta_T = 2$, $\beta = 0$, and $\phi = 1$.

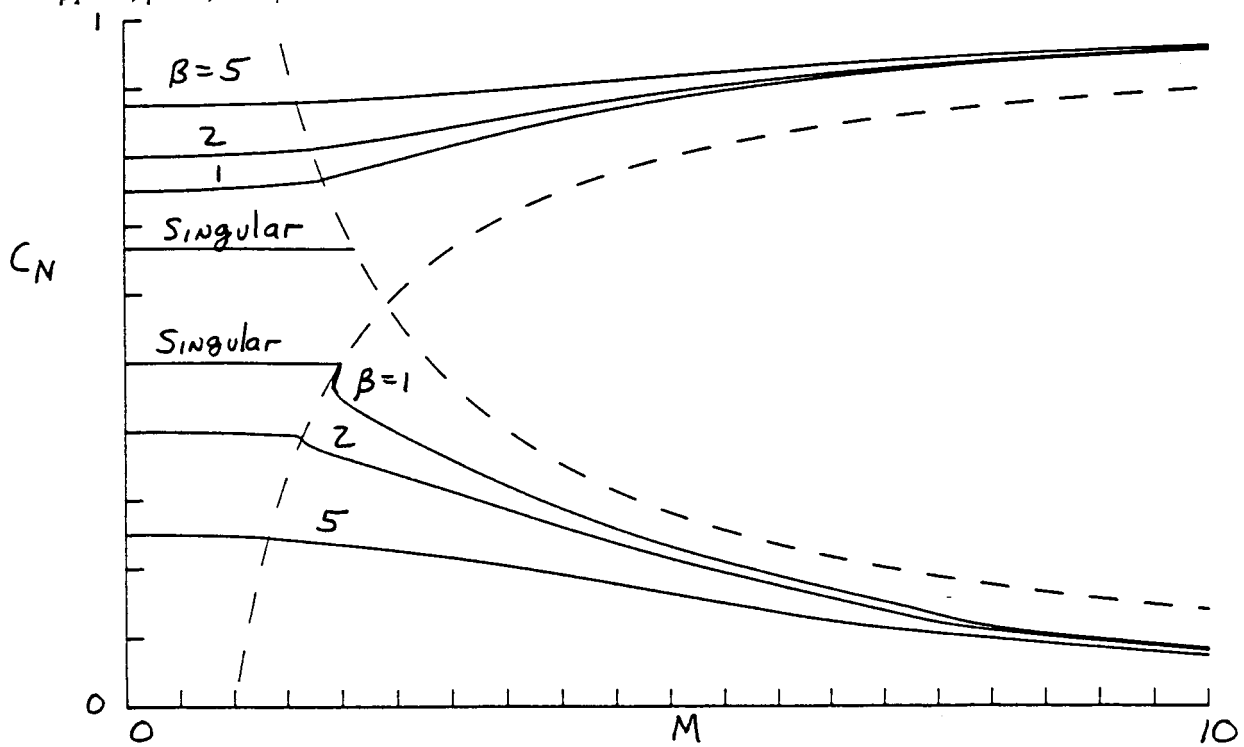


Figure 13b. Plot of neutral phase speeds (solid) and sonic speeds (dashed) versus Mach number for $\beta_T = 2$, $\beta = 1, 2, 5$, and $\phi = 1$.

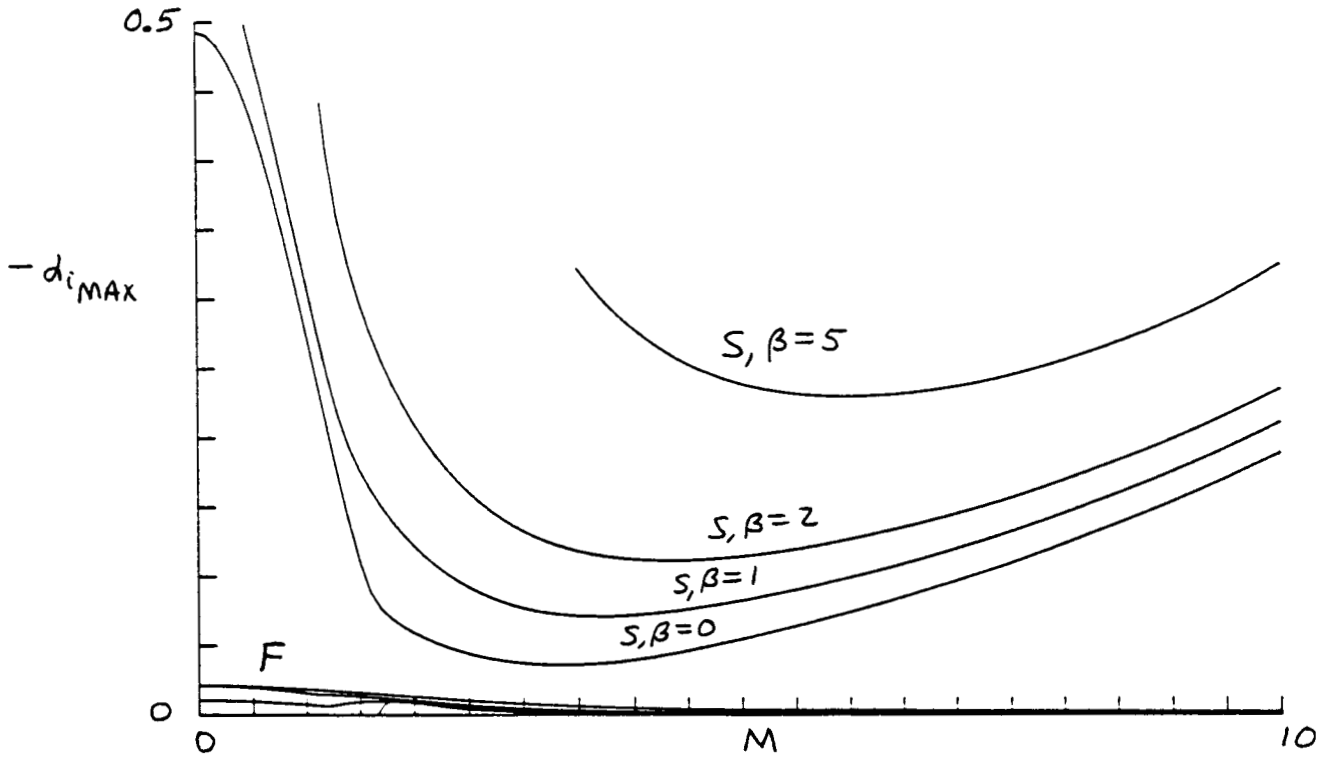


Figure 14a. Plot of maximum growth rates of the fast and slow modes versus Mach number for $\beta_T = 0.5$, $\beta = 0$, 1, 2, 5, and $\phi = 1$.

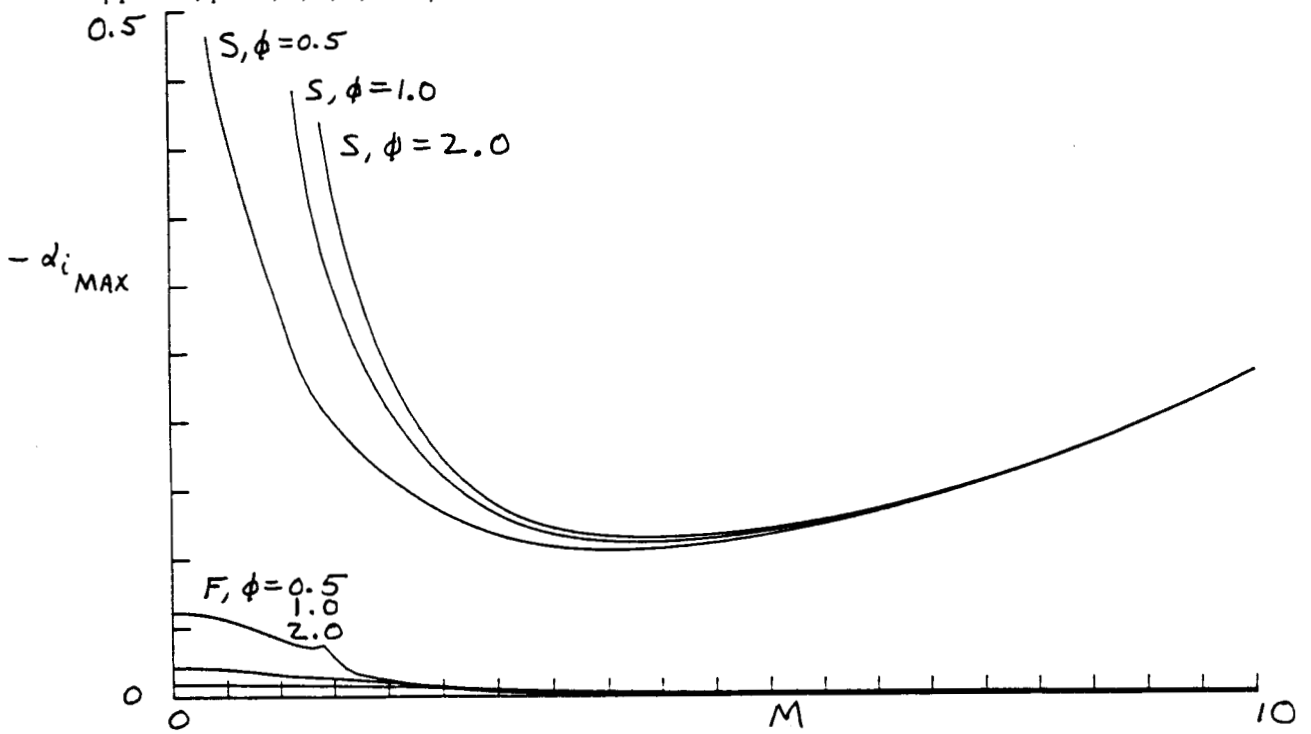


Figure 14b. Plot of maximum growth rates of the fast and slow modes versus Mach number for $\beta_T = 0.5$, $\beta = 2$, and $\phi = 0.5$, 1, 2.

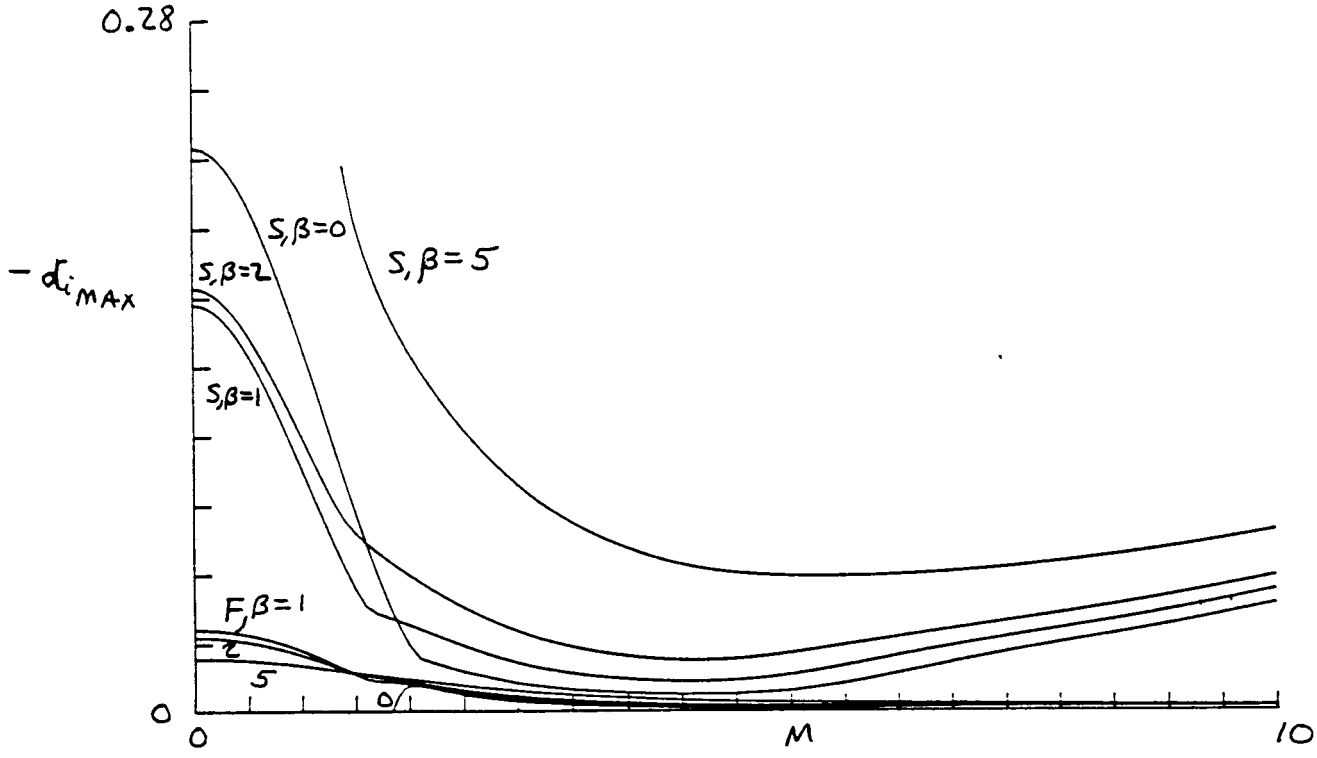


Figure 15a. Plot of maximum growth rates of the fast and slow modes versus Mach number for $\beta_T = 1$, $\beta = 0, 1, 2, 5$, and $\phi = 1$.

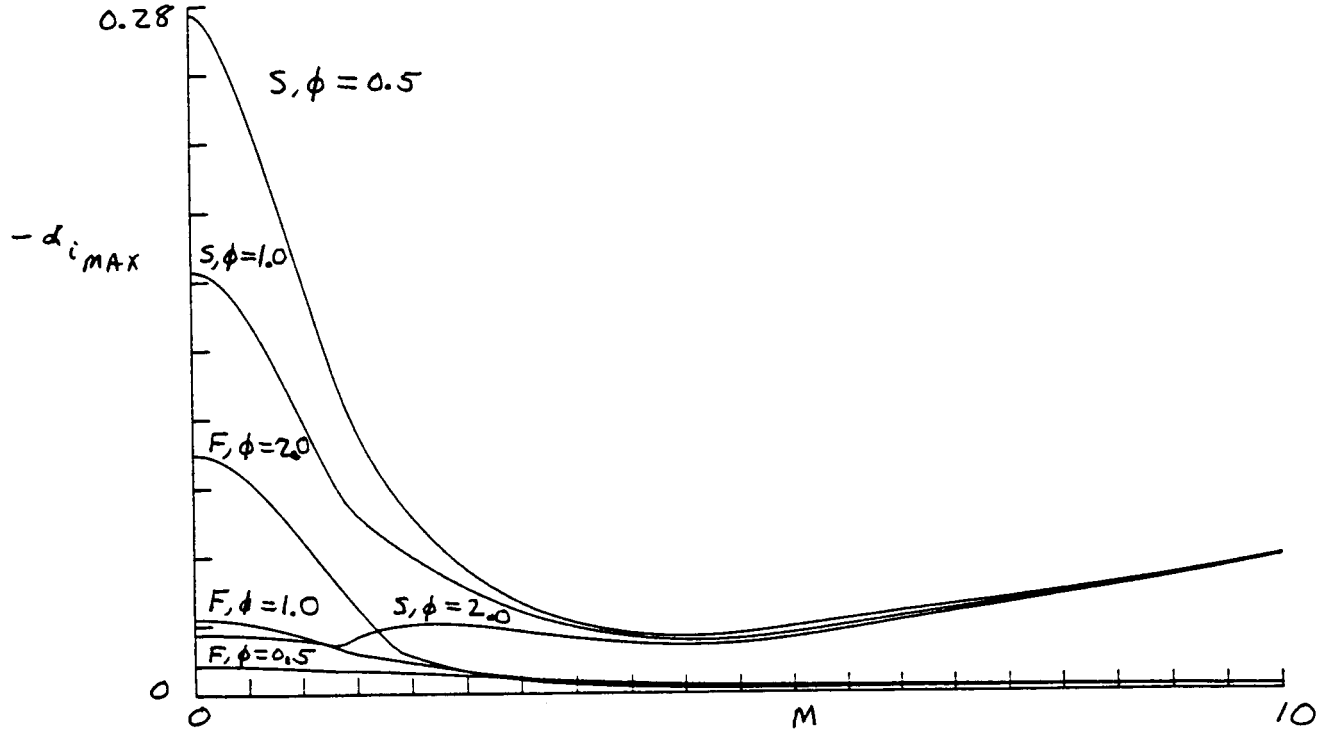


Figure 15b. Plot of maximum growth rates of the fast and slow modes versus Mach number for $\beta_T = 1$, $\beta = 2$, and $\phi = 0.5, 1, 2$.

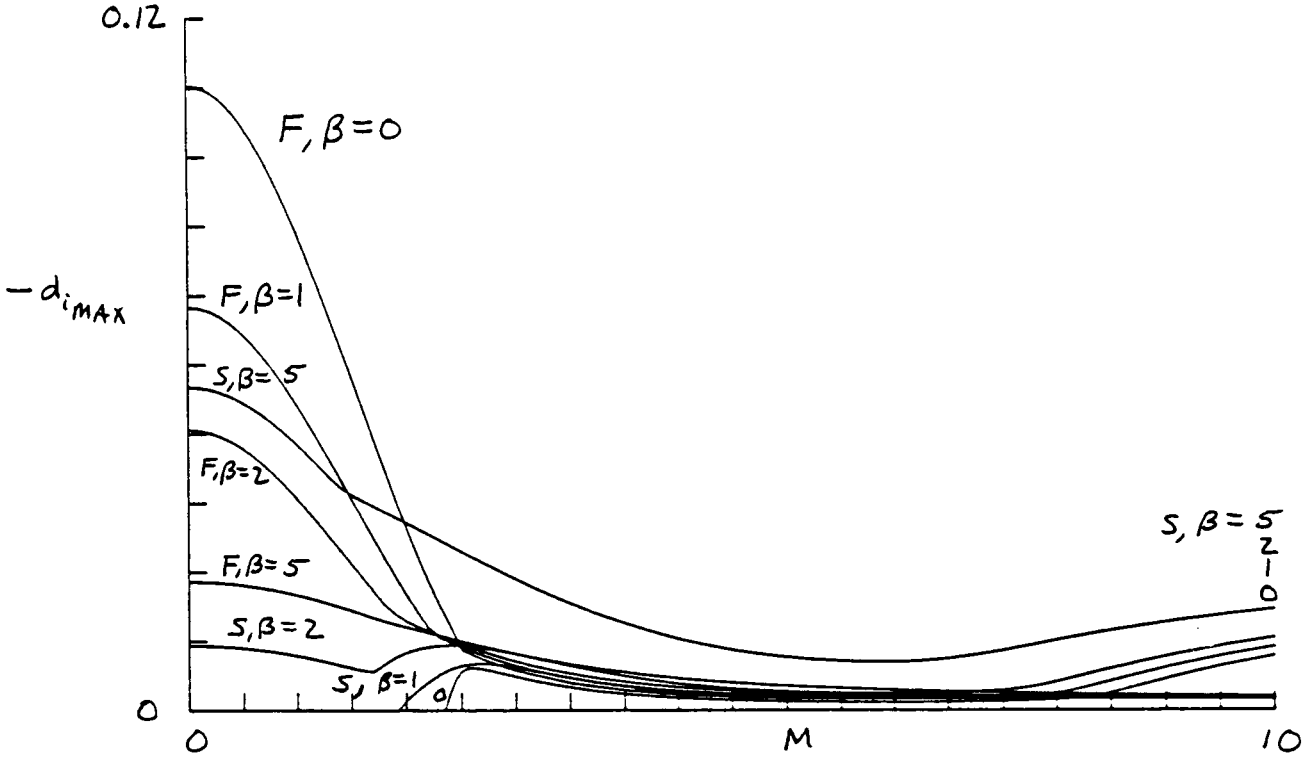


Figure 16a. Plot of maximum growth rates of the fast and slow modes versus Mach number for $\beta_T = 2$, $\beta = 0, 1, 2, 5$, and $\phi = 1$.

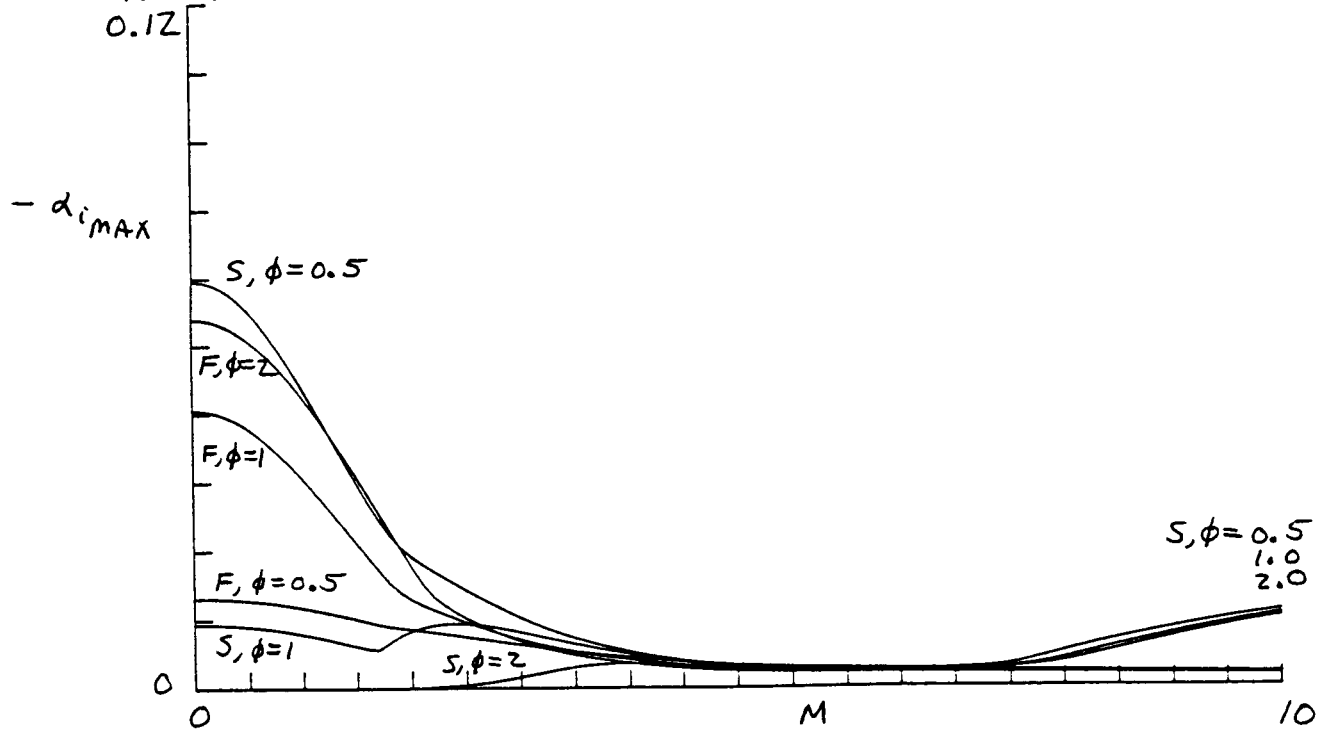


Figure 16b. Plot of maximum growth rates of the fast and slow modes versus Mach number for $\beta_T = 2$, $\beta = 2$, and $\phi = 0.5, 1, 2$.

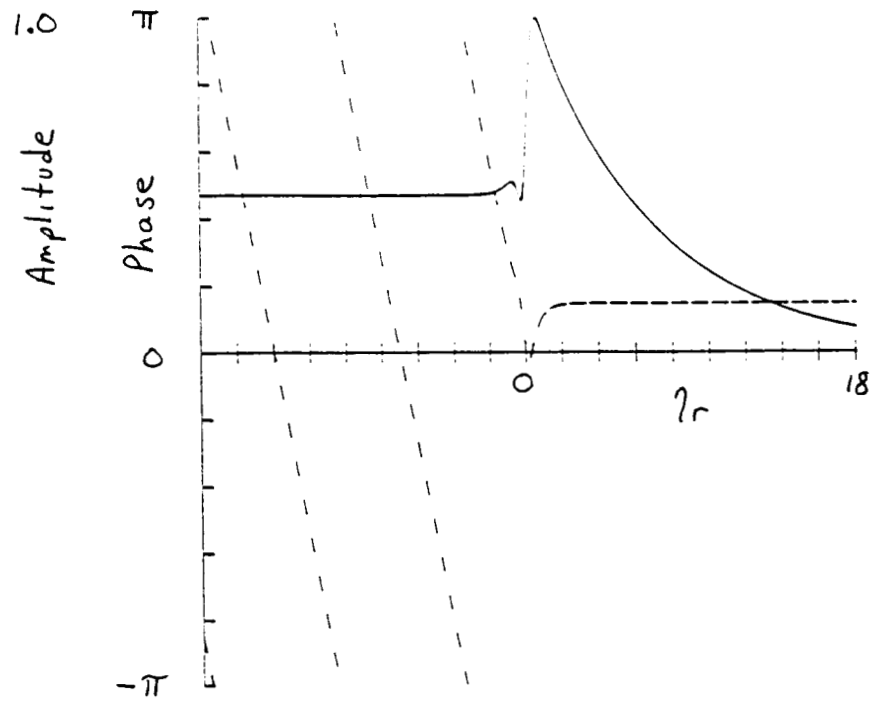


Figure 17. Plot of the two dimensional fast supersonic neutral eigenfunction $\Pi(\eta)$ along the contour $\eta = \eta_r - i$. The solid curve corresponds to the amplitude and the dashed curve to the phase. M = 5, $\beta_T = 1$, $\phi = 1$, $\beta = 0$, with $\omega_N = 0.184813$, $\alpha_N = 0.215661$, $c_N = 0.85696$.

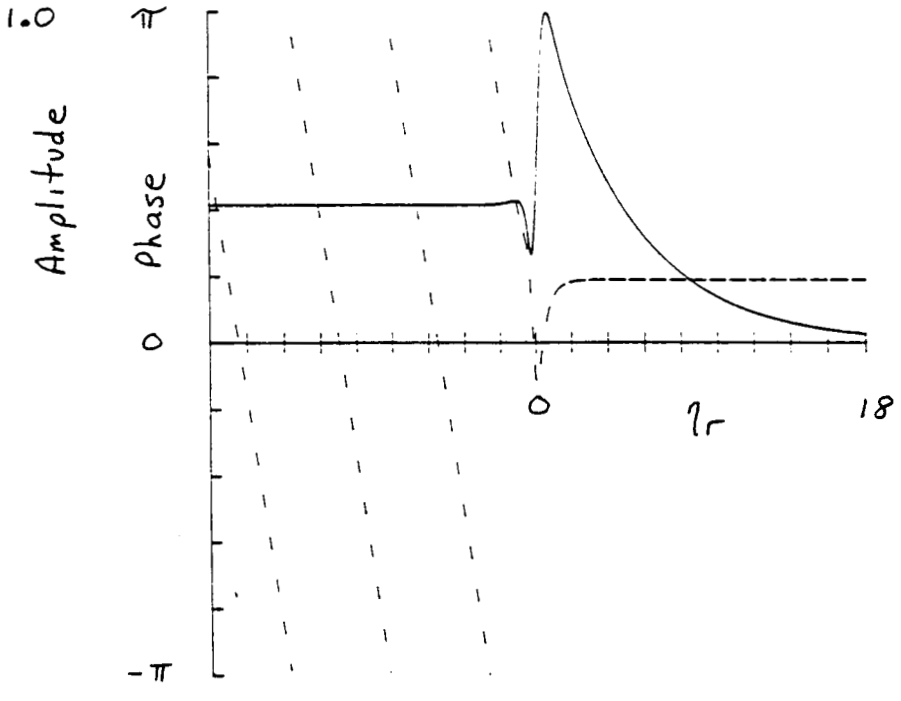


Figure 18. Plot of the two dimensional fast supersonic neutral eigenfunction $\Pi(\eta)$ along the contour $\eta = \eta_r - i$. The solid curve corresponds to the amplitude and the dashed curve to the phase. M = 5, $\beta_T = 1$, $\phi = 1$, $\beta = 1$, with $\omega_N = 0.235413$, $\alpha_N = 0.269485$, $c_N = 0.873565$.

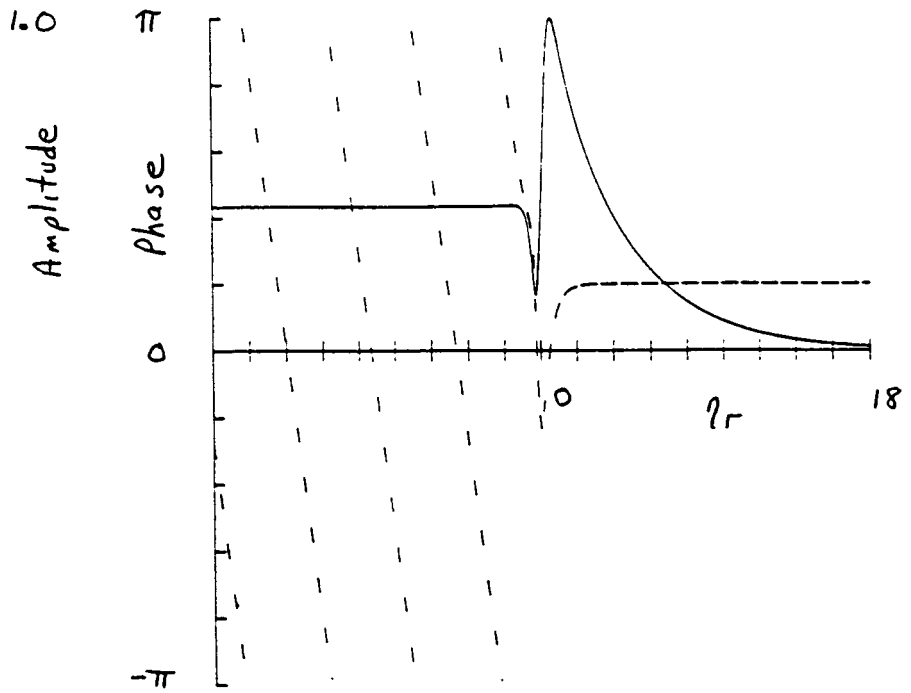


Figure 19. Plot of the two dimensional fast supersonic neutral eigenfunction $\Pi(\eta)$ along the contour $\eta = \eta_r - i$. The solid curve corresponds to the amplitude and the dashed curve to the phase. M = 5, $\beta_T = 1$, $\phi = 1$, $\beta = 2$, with $\omega_N = 0.276698$, $\alpha_N = 0.312299$, $c_N = 0.886001$.

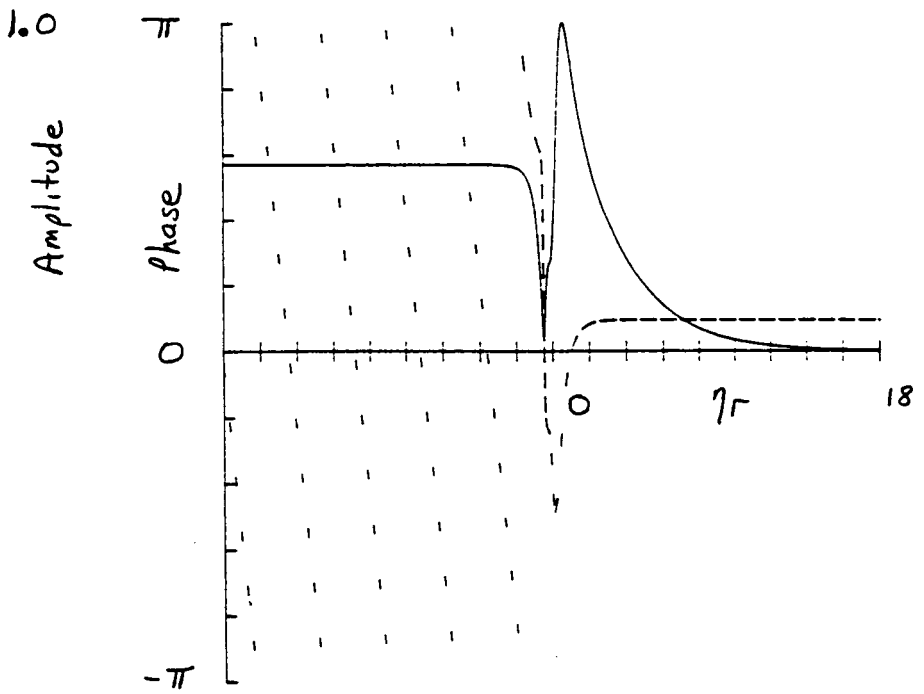


Figure 20. Plot of the two dimensional fast supersonic neutral eigenfunction $\Pi(\eta)$ along the contour $\eta = \eta_r - i$. The solid curve corresponds to the amplitude and the dashed curve to the phase. M = 5, $\beta_T = 1$, $\phi = 1$, $\beta = 5$, with $\omega_N = 0.356124$, $\alpha_N = 0.390535$, $c_N = 0.911887$.

NASA
National Aeronautics and Space Administration

# Report Documentation Page

| 1. Report No. | 2. Government Accession No. | 3. Recipient's Catalog No. |
|---|---|---|
| NASA CR-181815<br>ICASE Report No. 89-18 | | |

| 4. Title and Subtitle | 5. Report Date |
|---|---|
| INVISCID SPATIAL STABILITY OF A COMPRESSIBLE MIXING LAYER. PART II. THE FLAME SHEET MODEL | March 1989 |
| | 6. Performing Organization Code |

| 7. Author(s) | 8. Performing Organization Report No. |
|---|---|
| T. L. Jackson<br>C. E. Grosch | 89-18 |
| | 10. Work Unit No. 505-90-21-01 |

| 9. Performing Organization Name and Address | 11. Contract or Grant No. |
|---|---|
| Institute for Computer Applications in Science and Engineering<br>Mail Stop 132C, NASA Langley Research Center<br>Hampton, VA 23665-5225 | NAS1-18107<br>NAS1-18605 |
| | 13. Type of Report and Period Covered Contractor Report |
| 12. Sponsoring Agency Name and Address | 14. Sponsoring Agency Code |
| National Aeronautics and Space Administration<br>Langley Research Center<br>Hampton, VA 23665-5225 | |

15. Supplementary Notes

Langley Technical Monitor:
Richard W. Barnwell

Journal of Fluid Mechanics

Final Report

16. Abstract

We report the results of an inviscid spatial calculation for a compressible reacting mixing layer. The limit of infinitive activation energy is taken and the diffusion flame is approximated by a flame sheet. Results are reported for the phase speeds of the neutral waves and maximum growth rates of the unstable waves as a function of the parameters of the problem: the ratio of the temperature of the stationary stream to that of the moving stream, the Mach number of the moving stream, the heat release per unit mass fraction of the reactant, the equivalence ratio of the reaction, and the frequency of the disturbance. These results are compared to the phase speeds and growth rates of the corresponding nonreacting mixing layer. We show that the addition of combustion has important, and comlex, effects on the flow stability.

| 17. Key Words (Suggested by Author(s)) | 18. Distribution Statement |
|---|---|
| Inviscid spatial stability,<br>compressible, reacting,<br>flame sheet | 34 - Fluid Mechanics & Heat Transfer<br>59 - Mathematical Computer Sciences<br>Unclassified - Unlimited |

| 19. Security Classif. (of this report) | 20. Security Classif. (of this page) | 21. No. of pages | 22. Price |
|---|---|---|---|
| Unclassified | Unclassified | 32 | A03 |



NASA-Langley, 1989